THE ENERGY AND EFFECT OF IONIZATION ON CLUSTER FORMATION AND POST IONIZATION DYNAMICS OF ENERGETIC MATERIALS: A DENSITY FUNCTIONAL STUDY ON $(C_3H_6N_6O_6)_2$

by

Güven Kıyak

B.S., Chemistry, Anadolu University, 2007

Submitted to the Institute for Graduate Studies in
Science and Engineering in partial fulfillment of
the requirements for the degree of
Master of Science

Graduate Program in Chemistry

Boğaziçi University

2011

To my family

ACKNOWLEDGMENTS

I would like to express my most sincere gratitude to my thesis supervisor Assist. Prof. Fatma Ahu Akın for her endless attention and scientific guidance throughout this study. I appreciate her support and useful comments throughout the work.

I would extend my thanks to Prof. Viktorya Aviyente for her helpful and constructive review of the final manuscript.

I wish to express my thanks to Prof. Türkan Haliloğlu for her careful and constructive review of the final manuscript.

I thank my friends, Tugce Nihal Gevrek , Elif Kılıç İyilik, Özgül Gök, Saltuk Hanay, Eun Ju Park, Melike Eceoğlu, Nuray Yıldırım, Gamze Tanrıver, Pelin Ertürk, Nazlı Böke, Özlem İpek Kaloğlu, Sinem Kocaoğlan, Hasan Hüseyin İnce, Murat Burak Türk, Esra Bozkurt, Jesmi Çavusoğlu, Nergiz Cengiz for their companionship. I would like to thank the members of the faculty in Bogaziçi University Chemistry Department, especially Hülya Metiner for her invaluable helps.

Finally, my deepest thanks go to my whole family for their endless love, support and encouragement throughout these years.

This research has been supported by The Scientific and Technological Research Council of Turkey (TUBITAK) (110T485)

ABSTRACT

THE ENERGY AND EFFECT OF IONIZATION ON CLUSTER FORMATION AND POST IONIZATION DYNAMICS OF ENERGETIC MATERIALS: A DENSITY FUNCTIONAL STUDY ON $C_3H_6N_6O_6$

In this work, structures and energetics of $(C_3H_6N_6O_6)_2$ and $[(C_3H_6N_6O_6)_2]^+$ molecules have been investigated via computational chemistry methods. Using Density Functional Theory, the neutral and positively charged dimer structures of $C_3H_6N_6O_6$ have been calculated. The adiabatic and vertical ionization energies have been bracketed between 8 and 10 eV. The dominant dissociation pathways have been identified. Possibilities for further clustering have been investigated. A sum of 33 neutrals and 27 cations have been found. These structures coexist within an energy range of 30 kJ/mol. Cations are encountered in the form of charge-dipole complexes and proton-transfer complexes while the neutrals are brought together by long range dispersion forces.

ÖZET

YÜKSEK ENERJİLİ MADDELERDE ENERJİ, KÜMELENME OLUŞUMUNDA İYONİZASYON ETKİSİ VE İYONLAŞMA SONRASI DİNAMİKLER: $C_3H_6N_6O_6$ ÜZERİNE YOĞUNLUK FONKSİYONEL ÇALIŞMASI

Bu çalışmada $(C_3H_6N_6O_6)_2$ ve $[(C_3H_6N_6O_6)_2]^+$ molekül yapıları ve enerjileri hesapsal kimya yöntemleriyle incelenmiştir. Yoğunluk fonksiyonel teorisi kullanılarak nötr ve pozitif yüklü $C_3H_6N_6O_6$ dimer yapıları hesaplanmıştır. Yapılan hesaplamalar $C_3H_6N_6O_6$ molekülüne ait dimer yapılarının adiabatik ve dikey iyonlaşma enerjilerinin 8 ve 10 eV değerleri arasında değiştiğini göstermektedir. Dimer yapılarında gözlenen dominant ayrışma yolu gösterilmiştir. $C_3H_6N_6O_6$ molekülünün daha ileri düzeydeki kümelenme olasılıkları incelenmiştir. Bu çalışmada 33 nötr ve 27 katyon dimeri incelenmiştir. Bu dimer yapılarının enerjileri 30 kJ/mol aralığındadır. Katyonlarda ion-dipol ve proton transfer komplekslerine rastlanırken nötr dimerler dispersiyon kuvvetleriyle birarada tutulmaktadır.

TABLE OF CONTENTS

LIST OF FIGURES

LIST OF TABLES

LIST OF SYMBOLS

$E_{XC}[\rho]$	Exchange correlation energy
E_C^{VWN}	Vosko-Wilk-Nusair correlation functional
E_X^{B88}	Becke's Gradient correction
E_X^{exact}	Exact exchange energy
$V_{ee}[\rho]$	Interelectronic interaction energy
$F[\rho]$	Universal functional
$T[\rho]$	Kinetic energy of interacting electrons
$Ts[\rho]$	Kinetic energy of non-interacting electrons
$\rho(r)$	Electron density
$v_{eff}(\mathbf{r})$	Kohn-Sham effective potential
$v(r)$	External potential
$v_{xc}(\mathbf{r})$	Exchange correlation potential
$J[\rho]$	Coulomb energy
φ_i	Kohn-Sham orbitals
$E_X{}^{LDA}[\rho]$	Exchange functional
$\Delta E_X{}^{B88}$	Becke's gradient correction to the exchange functional
U_{xc}^{λ}	Exchange energy density

LIST OF ACRONYMS / ABBREVIATIONS

LDI	Laser desorption ionization
MALDI	Matrix assisted laser desorption ionization
B3LYP	Becke-3-parameter Lee-Yang-Parr functional
DFT	Density functional theory
LDA	Local density approximation
HF	Hartree-Fock theory
TOF-MS	Time of flight mass spectrometry
MPI	Multiphoton ionization
VUV	Vacuum Ultraviolet
TNT	2,4,6-Trinitrotoluene
BSSE	Basis Set Superposition Error

1. INTRODUCTION

1.1. Energetic Materials

The $C_3H_6N_6O_6$ is an important chemical agent as a result of its use in explosive materials and propellants [1]. This molecule is classified as an energetic molecule. Like all energetic molecules, its detection is of paramount importance. Such molecules, however, are difficult to detect as intact because they decompose by the slightest energetic stimulus as their ring structure is already strained and the N-N bonds are labile. In addition, they have low vapor pressure in solid solutions [2]. The $C_3H_6N_6O_6$ molecule consists of the three NO_2 groups bonded to the nitrogen atoms of a triazine ring (Figure 1.1). The conformers of $C_3H_6N_6O_6$ are distinguished mainly by the arrangement of nitro groups relative to the ring atoms of the $C_3H_6N_6O_6$ molecule.

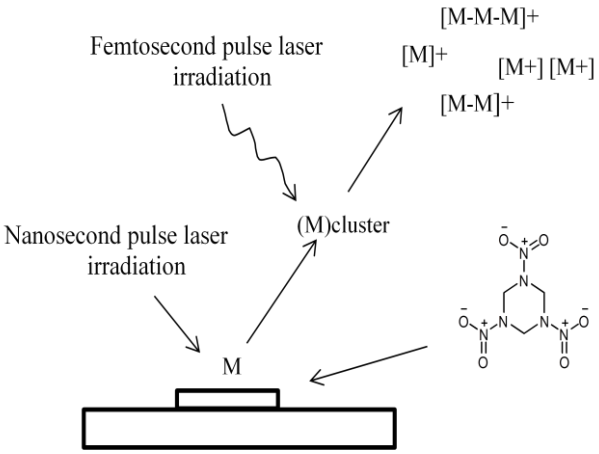

Figure 1.1. Shematic representation of the two step LDI.

During laser-desorption-ionization mass spectrometry (LDPI-MS) experiments, energetic molecules like the $C_3H_6N_6O_6$ molecule become reactive and decompose via electronic excitation or vibrational excitation due to interaction with the laser field. Quantitative analysis of the $C_3H_6N_6O_6$ molecule depends on the ability to keep the molecule intact during passage into the gas phase and ionization without overloading its

electronic, vibrational and rotational states with excess internal energy. Due to decomposition problems, the ionization energy of the intact $C_3H_6N_6O_6$ molecule could not be measured. The decomposition occurs faster than the detection timescales and decimates the heterocyclic ring thereby reducing the intensity of the $[C_3H_6N_6O_6]^+$ ion below the detection limits. It is therefore necessary to find a marker for molecular detection of $C_3H_6N_6O_6$ rather than fragments such as $[NO]^+$ that are common to all energetic compounds.

The calculation strategies followed in this work are closely related to the actual experimental detection process of the energetic materials. Being mostly in solid form or in solid mixtures, the compounds have to be brought into the gas phase by laser ablation, and ionized by multiphoton ionization by two separate lasers in two separate steps. Then the ions have to be detected by mass spectrometry. The fate of a molecule going through this treatment is described briefly below.

1.2. Laser Desorption Ionization

Laser Desorption (LD) is formation of gas-phase neutral species by the interaction of a pulsed laser with a solid or liquid material. The objective is to vaporize the sample material without fragmentation, often as a tool of sample introduction for mass spectrometry.

Laser Desorption Ionization (LDI) occurs when the sample directly absorbs energy from the laser and heats up via direct or secondary thermal changes, therefore generating desorbed ions. Both ablation and desorption occur simultaneously. In MALDI, a more commonly known variant of LDI, there is very little fragmentation however, this is only possible when analytes are mixed with a matrix [3]. The matrix absorbs the energy provided by the laser and delivers some of this energy to the analyte by non-radiative energy transfer. The most important drawback in MALDI is that the matrix is a magic concoction of laser absorbers and solvents which ultimately can enhance or suppress ion creation. It also is not suitable for off-site measurements [4-9].

When a surface is ablated, more neutrals are ejected than ions. To take advantage of this, LDI has been modified to separate the ablation and ionization processes. Two-step LDI requires two laser pulses. The first laser pulse ushers the sample into the vapor phase. Molecules in this vapor phase carry thermal energy dependent on the laser fluence and wavelength, their vibrational and electronic degrees of freedom, heat capacity, and the plume density. The second laser pulse is adjusted in energy and wavelength to study various photochemical responses or to create ions [13]. For this reason, any computational approach targeting ion structures should start with the identification of the neutrals.

1.2.1. Femtosecond Ionization/Dissociation

There are two ways that have been shown to create intact ions from the neutral molecules: multiphoton ionization (MPI) and ionization by a single vacuum ultraviolet (VUV) photon carrying around 10.5 eV energy. Nitro-compounds tend to dissociate quickly after photoexcitation by a nanosecond laser, which greatly reduces the probability for the absorption of the additional photons necessary for ionization. The resulting photofragments are not specific enough to identify the parent molecule. These two methods have been applied to energetic materials as the second step in the two-step analysis.

The major difference observed between the two time regimes was the detection of the parent molecular ion when femtosecond laser pulses were employed. It has been shown that femtosecond laser ionization is capable of producing parent ion and characteristic high-mass fragment ions for both organics [10] and inherently labile nitro-aromatic molecules [11-12]. Fragmentation is reduced and more chemospecific detection is possible. The reason lies in the difference between timescales of electronic motion and nuclear motion. In MPI the laser interacts with the molecules for a time interval which is shorter than the rotational timescales of molecules. The femtosecond pulse width of 100 fs or smaller is also appropriate for bypassing molecular dissociation channels and brings the molecule straight to the ionization continuum.

Single-photon ionization by a VUV laser with a photon energy of 10.5 eV is high enough to ionize all organic molecules in one step except methane, ethane and acetylene[14]. Given that the ionization potentials of most organic molecules lie between

7 and 13 eV, VUV sources can be considered as a “universal detector” [15, 16]. So VUV lasers can be seen as a possible soft-ionization source for organic compounds.

Once the neutrals are formed, the ions produced by either of the two techniques above will initially have the same geometry as the neutral since ionization occurs very fast compared to the geometrical rearrangements that follow it. Therefore the energy needed for ionization will be the vertical ionization energy which is the energy difference between the neutral and the cation of the same geometry. Vertical ionization sets the higher limit for ionization energy. The cation produced from the neutral will most likely change geometry to reach the nearest potential energy well. Its position on the multidimensional potential energy surface of the cation is determined by the neutral geometry. This in turn determines whether there are barrierless dissociation pathways on the cation energy landscape. If such pathways exist there will be high probability of fragmentation in the source or during flight time. In a computational strategy the neutral structure is computed, ionized and allowed to relax in subsequent steps. This provides a glimpse into these ionization and fragmentation processes and such a strategy is always employed in photoelectron spectroscopy studies.

1.3. Time-of-Flight Mass Spectrometry

In time-of-flight (TOF) mass spectrometry, ions of different m/z are dispersed in time during their flight along a field free drift path of a known length provided that all the ions start their journey at the same time [17]. The ions are then detected by an ion detector. Mass of the molecule or any molecular fragments can be determined by measuring the time of flight between ionization and detection; heavy ions travel slower than the small ions [11, 18-20]. The times of flight vary with the length of the flight tube and the accelerating voltages used in the instrument however, flight times around 10^{-6} seconds are typical. If an ion is detected after flight of such time length, it also means that the ion did not dissociate within that time. If parent ions are detected rather than fragments then it means that the previous ionization and ablation did not impart as much energy to allow fragmentation, and the cation that formed from the neutral was stable. Computationally, geometries of cations in situations where they are (i) locked at the neutral geometry, (ii) relaxed to cation potential energy minimum and, (iii) fragmented should all be considered. Flight-times of 10^{-6} seconds are too long compared to molecular internal vibrational relaxation and

dissociation timescales for labile molecules and any of the three situations could possibly occur.

1.4. Literature Work

Early experimental work on energetic compounds focussed on the unimolecular dissociation products of $C_3H_6N_6O_6$ upon thermal and electronic excitation, mechanisms of dissociation and dependence of the branching ratios of different mechanisms on experimental conditions. The 1970 mass spectrometry study of J. Stals [21] concentrated on the interaction of $C_3H_6N_6O_6$ with high energy electrons, $C_3H_6N_6O_6$ production, dissociation and identification of the dissociation products. The results indicated that thermal and photochemical ionization and electron impact yield similar ionic products. It was suggested that the decomposition occurs through different mechanisms due to strong molecular interactions in the solid form prior to ablation. The dissociation pathways of the $C_3H_6N_6O_6^+$ ion have been predicted by computational methods, taking the bonding characteristics and charge distributions into account. Later mass spectrometry studies of the thermal decomposition products of solid $C_3H_6N_6O_6$ [22, 23] showed that the $C_3H_6N_6O_6$ crystals decompose via four distincts pathways. It was suggested that after ionization into the $C_3H_6N_6O_6^+$ ion, the molecule dissociates through rearrangements initiated by the cleavage of the C-N, N-N, ve C-H bonds within the ring structure. This hypothesis was tested by studies employing different experimental methodologies [11, 24-33].

The recent simultaneous thermogravimetry controlled beam mass spectrometry, optical microscopy, time-lapse microscopy and scanning electron microscopy study of S. Maharrey and R. Behrens is the most thorough and instructive study on the thermal decomposition of $C_3H_6N_6O_6$ to date [31]. This study showed that at temperatures *below* the melting point of solid $C_3H_6N_6O_6$, decomposition initially occurs in the gas phase during sublimation. The gaseous decomposition products at the solid-air interface initiate new decomposition processes at the solid $C_3H_6N_6O_6$ surface by interacting with the surface molecules.

The computational studies on this topic initially focussed on the dissociation of thermally excited rather than ionized neutral nitroaromatic molecules [34-42]. The

$C_3H_6N_6O_6$ molecule has been one of the molecules studied. Dissociation mechanisms have been proposed based on the products observed during the mass spectrometry and infrared spectroscopy investigations since the observed decomposition products and their intensities have been different in each experimental study. The studies mentioned above did not correlate ion formation with the dimer formation.

Short-lived $[(C_3H_6N_6O_6)_n]^+$ cations have been observed in recent laser-desorption ionization mass spectrometry experiments [43]. Experimental variables such as laser light parameters, physical and chemical properties of the substrates from which the surface of which the $C_3H_6N_6O_6$ was desorbed, and the packing density of the solid $C_3H_6N_6O_6$ were found to affect the results. It is imperative that the problems of surface and gas-phase mechanisms for energy release and charge-transfer be tackled by a theoretical approach. Such studies are necessary to understand how experimental conditions will affect the detection of these heat sensitive compounds and achieve control of these conditions to maximize the molecular marker densities.

2. AIM OF THE STUDY

A wide variety of spectroscopic [46-48] and mass spectroscopic methods [11, 44, 45, 49] have been employed in probing energetic compounds but are limited to the detection of NO markers from the compounds in the mixture. A number of experimental and theoretical studies on the fragmentation pattern of $C_3H_6N_6O_6$ are reported [50]. However, there is a limited number of research on the cluster formation of $C_3H_6N_6O_6$.

Specifically, the potential of the neutral $(C_3H_6N_6O_6)_2$ cluster as a marker or a precursor to the molecular ion, $C_3H_6N_6O_6^+$ is of interest. Each $(C_3H_6N_6O_6)_2$ dimer could produce the ionized dimer or monomer $C_3H_6N_6O_6^+$ ion which is the molecular ion marker with m/z of 222 atomic mass units. Since there will be more degrees of freedom in a dimer than a monomer into which ablation energy can be partitioned, producing the marker via an indirect route could leave an internally cold and therefore detectable $C_3H_6N_6O_6^+$ ion for subsequent mass spectrometric investigation. It is therefore important to assess the possibility of the presence of the $(C_3H_6N_6O_6)_2$ complex in the ablation plume. Such a possibility could be determined computationally via calculation of the complexation energy of the complexes of monomer isomers and their interactions within the complex. It is also important to take formation of higher complexes such as $(C_3H_6N_6O_6)_3$ into consideration because this process reduces the quantity of the $(C_3H_6N_6O_6)_2$ complex.

The other important information is on the fate of the neutral dimer when it ionizes. If the neutral dimer is produced intact after ablation, ionization could cause decomposition. Based on how destructive the decomposition is, one may not observe dimer cation. Furthermore, monomer cation may not even be produced. Consequently, even though neutrals may be produced, the intact dimer or monomer ion signatures may diminish in the source or during the free flight in a mass spectrometer.

The objective of this thesis is to elucidate theoretically the structures of the $C_3H_6N_6O_6$ dimers and to investigate their presence as plausible markers in the detection of $C_3H_6N_6O_6$. The dominant intermolecular interactions responsible for dimer formation and the interactions observed in intact dimer cations have been investigated. From the

difference between the electronic and zero-point energies of the complexes and those of the individual monomer conformers, the complexation energies have been calculated. Vertical and adiabatic ionization energies have been calculated and compared to the monomer ionization energies. Possibility of higher complexation has been investigated by following the fate of dipole moments as the monomers become complexes. This study has been carried out by using density functional theory.

3. THEORY

3.1. Density Functional Theory

The basis for Density Functional Theory (DFT) is the proof by Hohenberg and Kohn that the ground state electronic energy is determined completely by the electron density ρ. In other words, there exist a one-to-one correspondence between the electron density of a system and the energy. Quoting directly from the Hohenberg-Kohn paper first theorem states that "the external potential $V_{ext}(\vec{r})$ is (to within a constant) a unique functional of $\rho(\vec{r})$; since in turn $V_{ext}(\vec{r})$ fixes $\hat{H}$ we see that full many particle ground state is a unique functional of $\rho(\vec{r})$.

The electron density is defined as:

$$\rho(x) = n \sum_{all\ m_s} \int .. \int |\psi(x, y, z, x_2, \dots, z_n, m_{s1}, \dots, m_{sn})|^2\, dx_2 \dots dz_n \quad (3.1)$$

$$\rho(\mathbf{r}) = n \sum_{all\ m_s} \int .. \int |\psi(\mathbf{r}, \mathbf{r}_2, \dots \mathbf{r}_n, m_{s1}, \dots, m_{sn})|^2\, d\mathbf{r}_2 \dots d\mathbf{r}_n \quad (3.2)$$

where m_s and x,y,z are the spatial coordinates of electrons. In Equation 3.2, the vector notation for the spatial variables is used [51].

According to the Hohenberg and Kohn [52] theorem an energy functional $E^0[\rho(r)]$ exists which achieves a minimum value for the exact ground state electron density $\rho^0(r)$

$$E^0[\rho] = \int v(\mathbf{r})\ \rho(\mathbf{r})\, d\mathbf{r} + F[\rho]\,, \quad (3.3)$$

$$F[\rho] = T[\rho] + V_{ee}[\rho] \quad (3.4)$$

$F[\rho]$ is a universal functional in which $T[\rho]$ represents the kinetic energy contribution and $V_{ee}[\rho]$ the electron-electron interaction term [53].

The importance of the Hohenberg-Kohn [52] theorem is best shown by comparing it with the wavefunction approach. A wave function for an N electron system contains 4N variables, three spatial and one spin coordinate for each electron. The electron density is the square of the wavefunction, integrated over N-1 electron coordinates, and each electron density only depends on three spatial coordinates independent of the number of electrons. While the complexity of a wave function increases exponentially with the number of electrons, the electron density has the same number of variables, independent of the system size. The only problem is that although it has been proven that each different density yields a different ground state energy, the functional connecting these two quantities is not known. The objective of DFT method is to find functionals connecting the electron density with the energy [54, 55].

A note on semantics: a function is a prescription for producing a number from a set of variables (coordinates). A functional is a prescription for producing a number from a function, which in turn depends on variables. A wavefunction and the electron density are thus functions, while the energy depending on a wave function or electron density is a functional.

The success of modern DFT methods is based on the suggestion by Kohn and Sham in 1965 that the electron kinetic energy should be calculated from an auxiliary set of orbitals used for representing the electron density [56]. The exchange correlation energy , which is a rather small fraction of the total energy, is then the only unknown functional, and even relatively crude approximations for this term provide quite accurate computational models. The simplest model is the local density approximation, where the electron density is assumed to be slowly varying, such that the exchange-correlation energy can be calculated using formulas derived for a uniform electron density. A significant improvement in the accuracy can be obtained by making the exchange correlation dependent also on the first derivative of the density, and further refinements also add the second derivative and mix Hartree-Fock exchange into the functional. Density functional theory is conceptually and computationally is very similar to Hartree-Fock theory , but provides much better results. The main problem in DFT is the inability to systematically improve the results and the known failure to describe certain important features, such as van der Waals interactions [57].

The foundation for the use of DFT methods in computational chemistry is the introduction of orbitals, as suggested by Kohn and Sham, 'KS' [56]. The idea in the KS formalism is to split the kinetic energy functional into two parts, one which can be calculated exactly and a small correction term. The price to be paid is that the orbitals are re-introduced, thereby increasing the complexity from 3 to 3N variables, and that electron correlation re-emerges as a separate term.

The key to Kohn-Sham theory is to calculate the kinetic energy under the assumption of non-interacting electrons [57]. The kinetic energy term for a noninteracting system is given by

$$T_S[\rho] = \sum_{i=1}^{N_{elec}} \left\langle \phi_i \left| -\frac{1}{2}\nabla^2 \right| \varphi_i \right\rangle \tag{3.5}$$

In order to separate the kinetic and exchange correlation terms the universal functional is written as

$$F[\rho] = T_S[\rho] + J[\rho] + E_{XC}[\rho] \tag{3.6}$$

The electronic energy may be rewritten as

$$E_{DFT}[\rho] = E_{ne}[\rho] + T_S[\rho] + J[\rho] + E_{XC}[\rho] \tag{3.7}$$

$$E_{XC}[\rho] \equiv (T[\rho] - T_S[\rho]) + (V_{ee}[\rho] - J[\rho]) \tag{3.8}$$

The $E_{XC}[\rho]$ term is called exchange correlation energy [52, 56]. The first parenthesis in Equation 3.8 may be considered as the kinetic correlation energy, while the last contains both potential correlation and exchange energy [57].

The Kohn sham effective potential is defined by

$$v_{eff}(\mathbf{r}) = v(\mathbf{r}) + \frac{\delta J(\rho)}{\delta \rho(\mathbf{r})} + \frac{\delta E_{XC}(\rho)}{\delta \rho(\mathbf{r})} = v(\mathbf{r}) + \int \frac{\rho(r')}{|r - r'|} dr' + v_{xc}(r') \tag{3.9}$$

With the exchange correlation potential equal to

$$v_{xc}(\mathbf{r}) = \frac{\delta E_{XC}(\rho)}{\delta \rho(\mathbf{r})} \tag{3.10}$$

Therefore for a given $v_{eff}(\mathbf{r})$ one obtains the $\rho(\mathbf{r})$ by solving the N one electron equations

$$\left[-\frac{1}{2}\nabla^2 + v_{eff}(\mathbf{r})\right]\varphi_i = \varepsilon_i \varphi_i \tag{3.11}$$

The independent orbitals φ_i are known as Kohn-Sham orbitals and give the exact density by

$$\rho(\mathbf{r}) = 2\sum_{i=1}^{N/2}\left|\varphi_i(\mathbf{r})\right|^2$$

if the exact form of this functional is known. However , the exact form of this functional is not known and approximate forms are developed starting with the Local Density Approximation. The exchange functional is given by

$$E_X{}^{LDA}[\rho] = -C_X \int \rho(\mathbf{r})^{4/3}\, dr \tag{3.12}$$

with C_X being a constant.The LDA method underestimates the exchange energy by about 10 per cent and does not have the correct asymptotic behavior.

One of the earliest and most popular Generalized Gradient Approximation (GGA) exchange functional was proposed by A. D. Becke (B88) as a gradient corrected functional

$$E_X{}^{B88} = E_X{}^{LDA} + \Delta E_X{}^{B88} \tag{3.13}$$

$$\Delta E_X{}^{B88} = -\beta \rho^{1/3}\, \frac{x^2}{1+6\beta x \sinh^{-1} x} \tag{3.14}$$

$$x = \frac{|\nabla\rho|}{\rho^{4/3}}$$

The β parameter is determined by fitting to known data for the rare gas atoms using the dimensionless gradient variable *x*. The B88 exchange functional has the correct asymptotic behavior for the energy density, but not for the exchange potential [58]. It reduces the error in the exchange energy by almost two orders of magnitude and thus represents a substantial improvement for a simple functional form containing only one adjustable parameter.

The adiabatic connection formula connects the non-interacting Kohn-Sham reference system (λ =0) to the fully-interacting real system (λ =1) and is given by

$$E_{XC} = \int_0^1 U_{xc}^{\lambda}\, d\lambda \qquad (3.15)$$

where λ is the interelectronic coupling-strength parameter and U_{xc}^{λ} is the potential energy of exchange-correlation at intermediate coupling strength. The adiabatic connection formula can be approximated by

$$E_{XC} = \frac{1}{2} E_x^{exact} + \frac{1}{2} U_{xc}^{LDA} \qquad (3.16)$$

Since$U_{xc}^{0} = E_x^{exact}$, the exact exchange energy of the Slater determinant of the Kohn-Sham orbitals, and $U_{xc}^{1} = U_{xc}^{LDA}$ [59].

The closed shell Lee-Yang-Parr(LYP) correlation functional [60] is given by

$$E_c = -\int \frac{1}{1 + d\rho^{-1/3}} \left\{ \rho + b\rho^{-2/3} \left[C_F \rho^{5/3} - 2t_w + \left(\frac{1}{9} t_w + \frac{1}{18} \nabla^2 \rho \right) \right] e^{-c\rho^{-1/3}} \right\} dr$$

(3.17)

$$t_w = \frac{1}{8} \frac{|\nabla\rho(r)|^2}{\rho(r)} - \frac{1}{8} \nabla^2$$

The mixing of LDA, B88, E_x^{exact} and the gradient-corrected correlation functional to give the hybrid functional [61] involves three parameters.

$$E_{XC} = E_{xc}^{LDA} + a_0 (E_x^{exact} - E_x^{LDA}) + a_x \Delta E_X{}^{B88} + a_c \Delta E_c{}^{non-local} \quad (3.18)$$

where $\Delta E_X{}^{B88}$ is the Becke's gradient correction to the exchange functional. In the B3LYP functional, the gradient-correction ($\Delta E_c{}^{non-local}$) to the correlation functional is included in LYP. However, LYP contains also a local correlation term which must be subtracted to yield the correction term only.

$$\Delta E_c{}^{non-local} = E_c^{LYP} - E_c^{VWN} \quad (3.19)$$

where E_c^{VWN} is the Vosko-Wilk-Nusair correlation functional, a parameterized form of the LDA correlation energy based on Monte Carlo calculations. The empirical coefficients are *a0*=0.20, *ax*=0.72 and *ac*=0.81 [62].

3.2. Basis Sets

A basis set is the set of mathematical functions from which the wave function is constructed. Each molecular orbital in the HF theory is expressed as a linear combination of basis functions. The full HF wave functions expressed as a slater determinant formed from the individual occupied molecular orbitals.In the abstract,the HF limit is achieved by use of an infinite basis set, which necessarily permits an optimal description of the electron probability density. In practice, however, one cannot make use of an infinite basis set.Thus much work has gone into identifying mathematical functions that allow wave functions to approach the HF limit arbitrarily closely in as efficient a manner as possible [63]. There are two types of set of basis functions for atomic Hartree-Fock calculations, Slater-type functions and Gaussian-type functions.

Standard basis sets for electronic structure calculations employ linear combinations of Gaussian functions to form the orbitals. Basis sets assign a group of basis functions to each atom within a molecule in order to approximate its orbitals. These basis functions themselves are composed of a linear combination of Gaussian functions,such basis functions are referred to as contracted functions, and the component gaussian functions are referred to as primitives. A basis function consisting of a single Gaussian function is named uncontracted.

Gaussian functions are closely related to exponential functions, which are of the form of exact solutions to the one-electron hydrogen atom, and comprise a polynomial in the Cartesian coordinates (*x*, *y*, and *z*) followed by an exponential in r^2.

Basis sets are classified according to the number and types of basis functions that they contain. Generally, larger basis sets impose fewer constraints on electrons and more accurately approximate exact molecular orbitals [64, 65].

3.2.1. Minimal Basis Sets

Minimal basis sets contain minimum number of basis functions needed for each atom and they use fixed-size atomic-type orbitals. The STO-3G basis set is a minimal basis set. It uses three Gaussian primitives per basis function which accounts for the ‘3G’ in its name. In addition, “STO” stands for ‘Slater type orbitals’, implying that STO-3G basis set approximate Slater orbitals with Gaussian functions [64].

3.2.2. Split Valence Basis Sets

Split valance basis sets are larger basis sets than minimal basis sets, in which the number of basis functions per atom are increased. Split valance basis sets represent core atomic orbitals by one set of functions and valance atomic orbitals by two sets of functions. For this purpose, hydrogen is provided by two s-type functions, and main-group elements are provided two sets of valance s- and p-type functions.

3-21G and 6-31G basis sets are the simplest ones among the split valance basis set, having two sizes of basis functions for each valance orbital. In the case of 3-21G split valance basis set, each core atomic orbital is expanded in terms of three Gaussians and also two and one Gaussians for inner and outer valance atomic orbitals, respectively. 6-31G basis sets are constructed in a similar manner, with core orbitals represented in terms of six

Gaussians and valance orbitals split into three and one Gaussian components Split-valence basis set splits only the valence orbitals in this way, whereas double zeta basis also have split core orbitals.

The double zeta basis sets, such as Dunning-Huzinaga basis set (D95) form all molecular orbitals from linear combinations of two sizes of functions for each atomic orbital. use linear combinations of two sizes of functions for each atomic orbital to form the molecular orbitals. Similarly, triple zeta basis sets, such as 6-311G, use three sizes of contracted functions for each orbital type, being written in terms of three, one and one Gaussians, respectively [64, 65].

3.2.3. Polarized Basis Sets

Polarized basis sets add orbitals with angular momentum what is required for the ground-state to the description of each atom. Thus, polarized basis sets allow orbitals to change their shape. In polarized basis sets, d functions are added to all heavy atoms is designated with a '*' or '(d)' and f functions to transition metals. Polarization can be added to hydrogen atoms as well, this would be done by '**' or '(d,p)'.

6-31G* (6-31G(d)), 6-31G** (6-31G(d,p)), are among the simplest polarized basis sets. Both 6-31G* and 6-31G** polarized basis sets are constructed from 6-31G basis set, by adding a set of d-type polarization functions to heavy (non-hydrogen) atoms in the former one and by adding p functions to hydrogen atoms in addition to the d functions on heavy atoms in the latter one [64].

3.2.4. Diffuse Functions

Diffuse functions are large-size versions of s- and p-type functions as opposed to the standard valence-size functions. They allow orbitals to occupy a larger region of space. Basis sets with diffuse functions are important for systems where electrons are relatively far from the nucleus: molecules with lone pairs, anions and other systems with significant negative charge, systems in their excited states, and systems with low ionization potentials,description of absolute acidities, and so on.

In such situations, basis sets are needed to be supplemented by diffuse s- and p-type functions on either heavy atoms designated by '+' or hydrogen atoms designated by '++'. The 6-31+G (d) basis set is the 6-31G (d) basis set with diffuse functions added to heavy atoms. The double plus version, 6-31++G (d), adds diffuse functions to the hydrogen atoms as well [64].

4. METHODOLOGY

The geometries of the $C_3H_6N_6O_6$ dimers were calculated by Becke3-Lee-Yang-Parr (B3LYP) hybrid density functional level of theory using the 6-31+G(d,p) basis set. The conformational preferences of the monomers relative to each other were chosen according to both dipole moment approach and Frontier Orbital approach. All of the calculations in this study were performed by using the Gaussian 03 program [66].

The first phase of the processes which are followed throughout this study are illustrated schematically in Figure 4.1. Initially the homodimers are brought together in combinations of I-I, II-II, and III-III by taking into dipole moment approach and frontier orbital approach. The geometries were fully optimized at the B3LYP/6-31+G(d,p) level. All dimers in this study were in their ground electronic states. Frequencies were calculated to confirm that the structure was a local or global minimum. Unless reported otherwise, the sum of the electronic and zero-point energies calculated at this level were used to calculate the complexation energies and the ionization potentials. Molecular orbitals calculated at this level were also reported.

The complexation energies were calculated using the electronic energies of neutral dimers corrected for the basis set superposition error (BSSE). The largest magnitude of complexation energy is around 40 kJ/mol and the maximum BSSE error is about 10 kJ/mol, 25% of the complexation energy, and could cause errors in energy ordering and stability arguments.

The second part of this study consisting of cation optimizations of these dimers are illustrated schematically in Figure 4.2. The cations were prepared by removing an electron from the highest occupied molecular orbital of the corresponding neutral wavefunctions. In order to calculate the vertical detachment energies, a frequency calculation of the cation at the neutral geometry was run to produce the zero-point corrected electronic energy of the cation. Using the forces of this step, the cation geometry was allowed to relax to a local

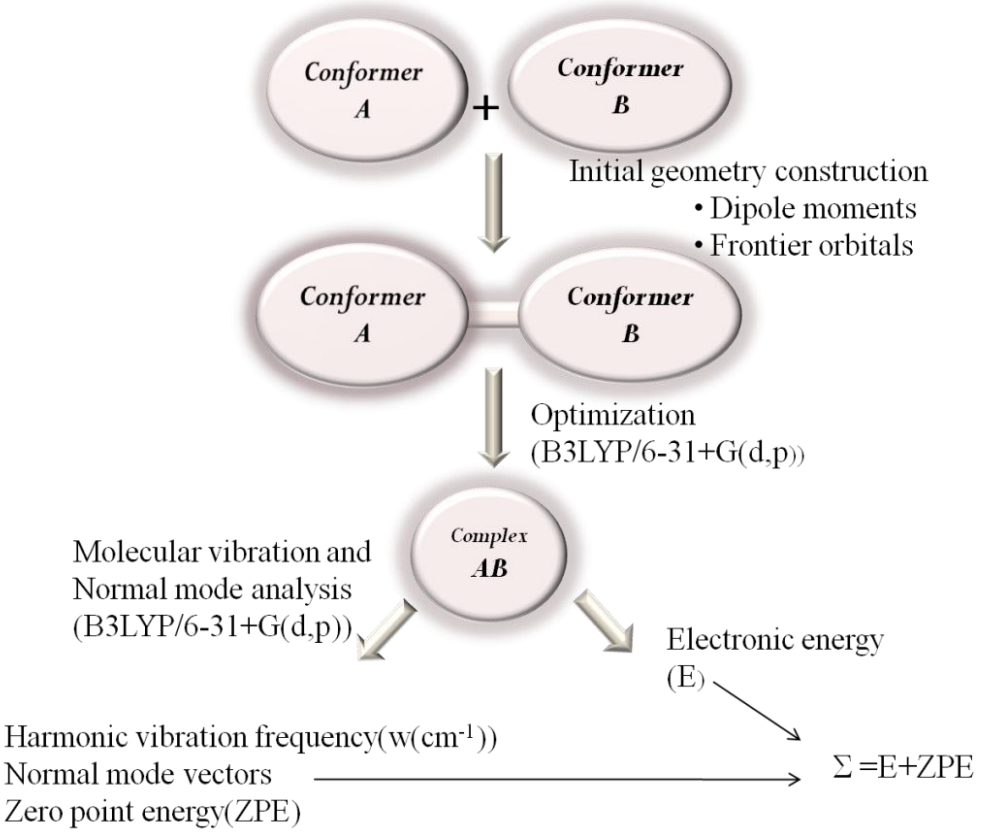

Figure 4.1. The schematic representation of the first step of the methodology used.

minimum which was confirmed by frequency calculations. Optimization of the cations of these dimers were performed to reach the local (or global) energy minimum of the cation and to calculate the adiabatic ionization energies. Adiabatic Ionization Energies (IE_{ad}) and Vertical Ionization Energies (IE_v) were calculated according to the Equation 4.1 and Equation 4.2 respectively.

$$IP_a = (T_0 + ZPE)_{M^+} - (T_0 + ZPE)_M \quad (4.1)$$

In Equation 4.1, M represents the neutral M molecule at its local minimum geometry. In a similar manner M^+ represents M^+ cation at its local minimum geometry, $M^+(R:M)$ represents M^+ cation at the local minimum geometry of the neutral in Equation 4.2.

$$IP_v = (T_0 + ZPE)_{M+(R:M)} - (T_0 + ZPE)_M \quad (4.2)$$

The atomic charges for the neutrals and the cations were calculated using the ChelpG [67] algorithm in the G03 program [66] at the B3LYP/6-31+G(d,p) level. The dipole moments reported by the ChelpG were used for analysis since they were derived from electrostatic potentials calculated by this algorithm.

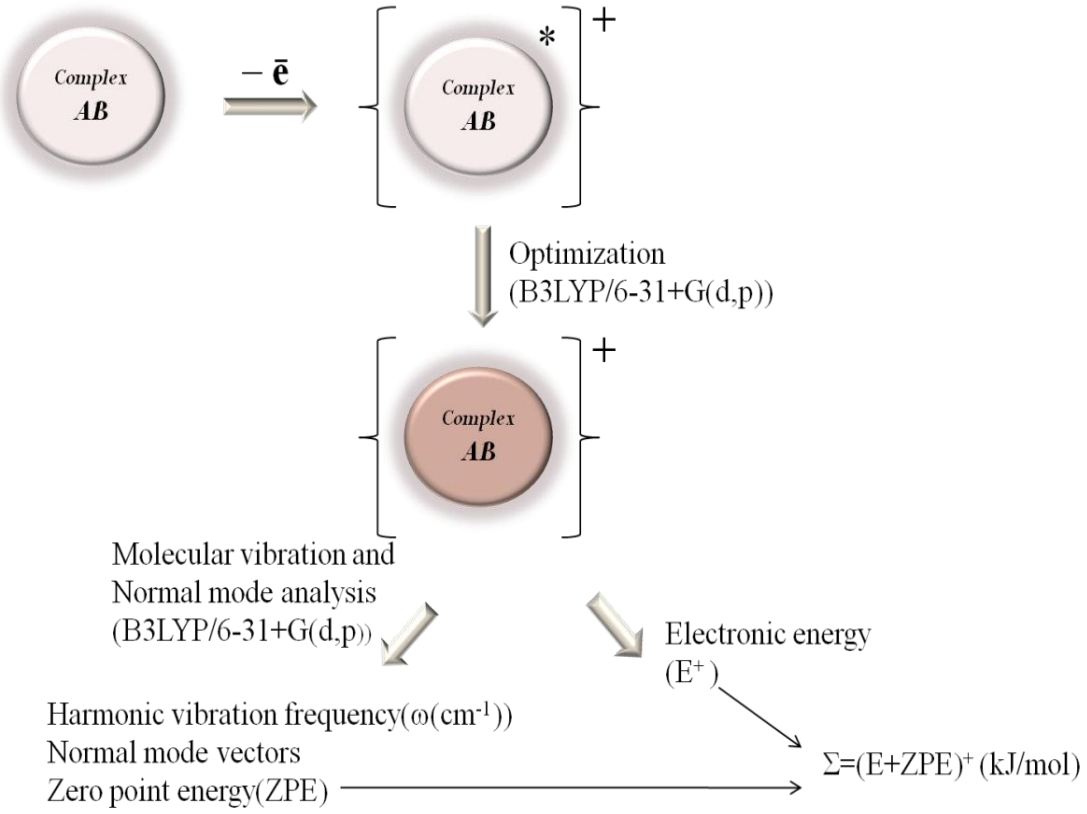

Figure 4.2. Schematic representation of the second step of the methodology used.

4.1. Generating Complex Structures: Dipole Moment Approach

In dipole moment approach, the two conformers of the $C_3H_6N_6O_6$ molecules were brought into close proximity by aligning them along their dipole moments. These conformers are displayed in Figure 4.3a. The geometries were optimized at the B3LYP/6-31+G(d,p) level and the dipole moments were calculated at these geometries using the same basis set.

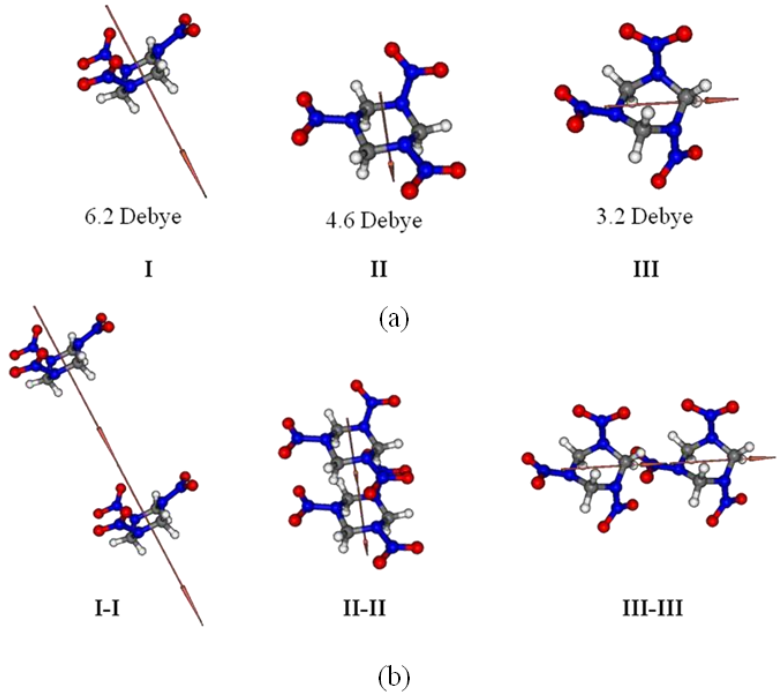

Figure 4.3. (a) Isomers and their dipole moments and (b) positioning according to dipole moment approach.

4.2. Generating Complex Structures: Frontier Orbital Approach

In Frontier Orbital approach HOMO-LUMO interaction of these isomers are taken into account. The HOMO orbital of one isomer and the LUMO orbital of another were brought together at different combinations regardless of how dominant or small each atom contributed to the molecular orbital.

The minimum energy $C_3H_6N_6O_6$ conformers which are used in this study were determined by Akin and are shown in Figure 4.5. Even though the three lowest energy conformers were used, conformers IV and V were also encountered as part of the dimers after the optimizations.

Most of the calculations were run on a HPZ800 workstation with 8 Intel Xeon processors at 3.07 GHz with a total of 64 Gb memory operating over a 500 Gb hard disk space.

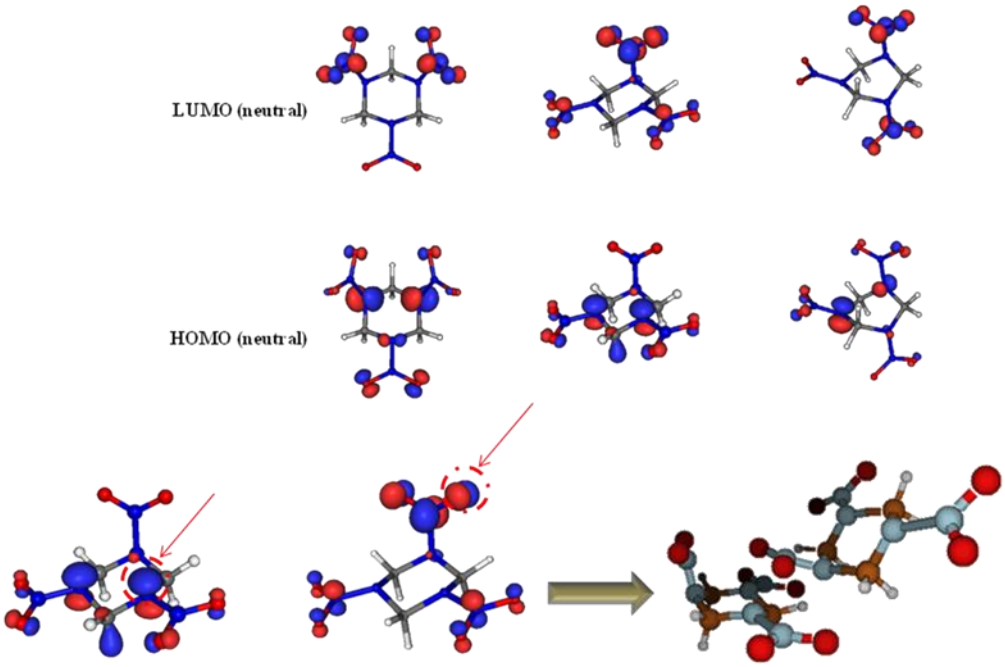

Figure 4.4. At the top, HOMO and LUMO orbitals of each isomer. At the bottom, Frontier orbital approach.

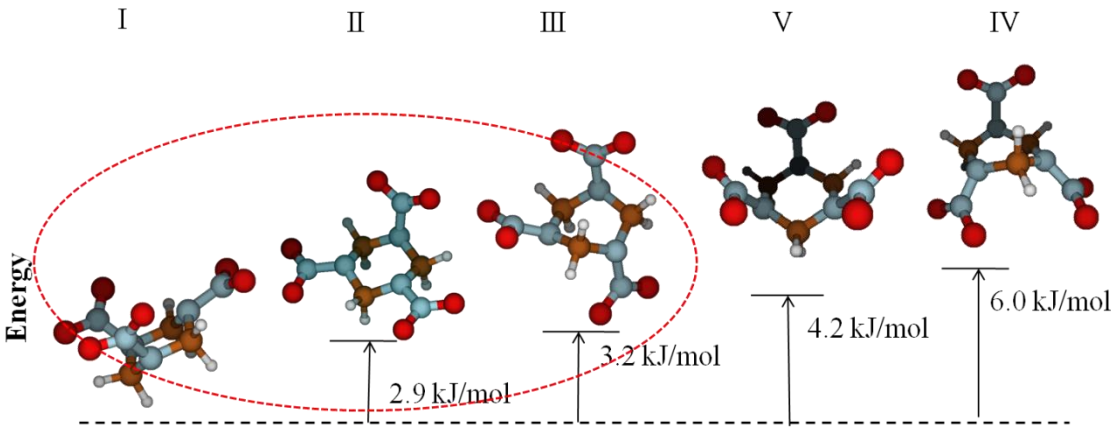

Figure 4.5. The $C_3H_6N_6O_6$ conformers. The conformers in the red circle are used in dimer configurations.

5. RESULTS AND DISCUSSION

5.1. Structures of neutrals and cations

The geometries of neutral $(C_3H_6N_6O_6)_2$ are shown in Figure 5.1. By combination of the same (homodimer) and different (mixed dimers) monomers, 33 of the attempted dimer configurations reached a minimum. All dimers are held together by long-range electrostatic interactions, namely, dipole-dipole interactions since all isomers have non-zero dipole moments. The complexes that remained isomerically intact during optimization are II-IIa, II-IIc, II-II2z, II-IIv, II-IIq, II-II5, III-III4, III-III1, I-I4, I-I7, I-I8, I-Ik, I-IIb, I-III, II-Ia, II-Ib, II-Ic, and II-IIIa. The dimers in the same class (I-I, II-II, III-III, II-I with the above lettering) differ by rotational isomerism only. Keeping one isomer fixed in space, these complexes are different by the position and angle of one isomer with respect to the other.

The dimers that went through isomeric "scrambling" had one isomer transform into another, with the exception of III-III9. In dimers II-II4 and II-IIw, one of the monomers isomerized to V and I, respectively. In I-IIa dimer, monomer I which is the lowest energy conformer in the set converged to V. In I-IIIb only one monomer changed its conformation to IV. In III-Ia and III-Ic, monomer III changed into conformer IV. In II-IIIb, II-IIId and III-IIa, one monomer is converted to IV. In II-IIIe, one of the monomers changed to isomer I. The isomer that went through transformation the most often was III. During optimization, monomer III isomerized into the more symmetrical albeit less stable isomer IV. In III-III3 dimer, only one of the monomers changed into IV. In dimers III-III7 and III-III9 both monomers changed into IV.

In the neutral complexes, it was observed that O (ONO) of one monomer and H (CH_2) of the other are the closest atoms and can get as close as 2.4 Å (between III of one dimer and IVof the other). However neither the C-H bonds are elongated nor a linear O-H-C relation exists to state the presence of H-bonding. The bond lengths in the neutral complexes are shown in Table 5.1

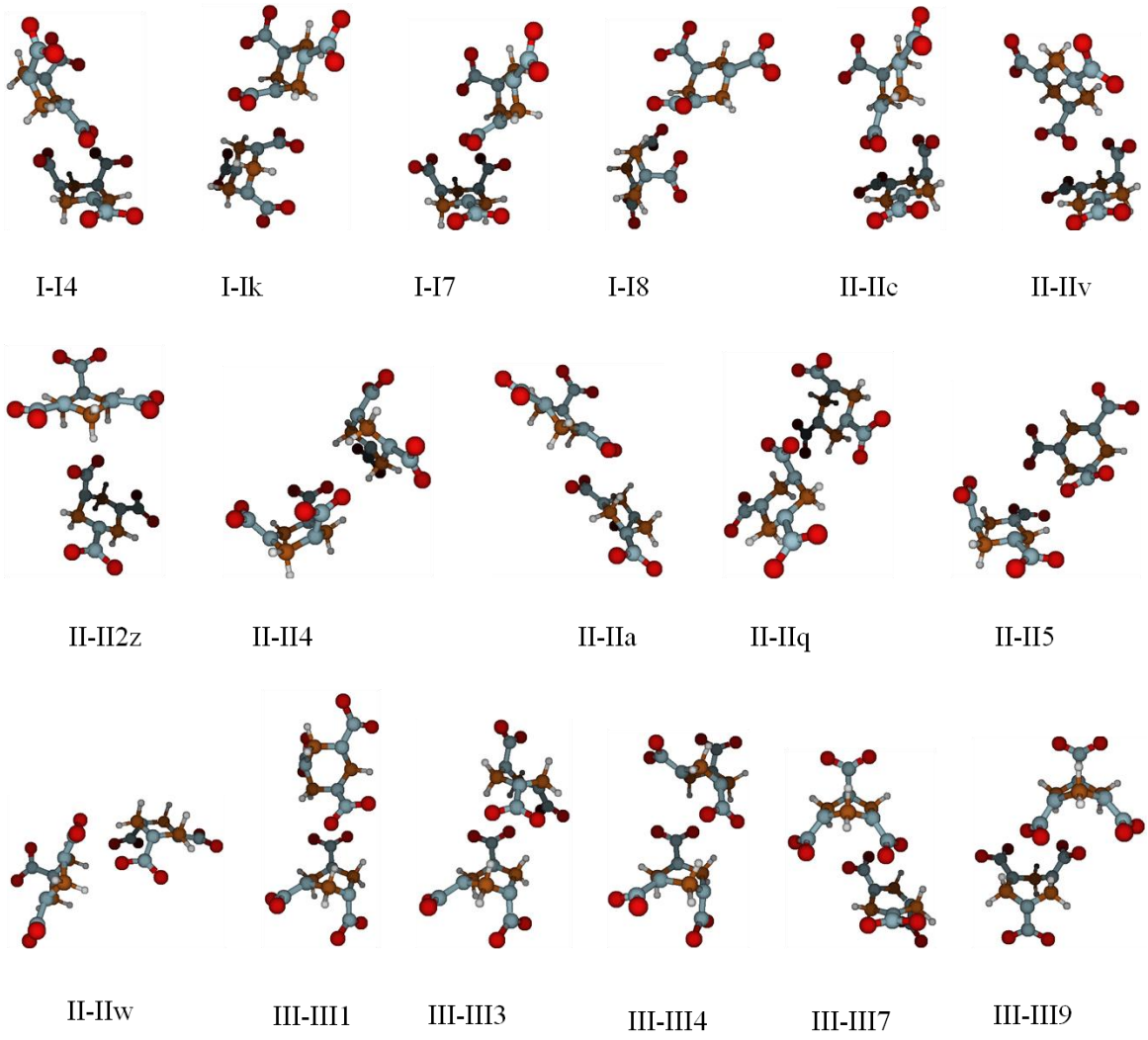

Figure 5.1. Optimized geometries of neutral dimers.

There is a reverse correlation between the N-N bond and the C-N bond lengths in the N-N-C triatomic moiety in all type of monomers that are used. As the N-N bond gets shorter, the C-N bond is extended and vice versa. A similar observation can be made about the O-N-N moieties. In addition, the C-H bond length also correlates with the intramolecular O-H bond distance.

In order to calculate ionization energies, ground state structures of the cations are as essential as those of the neutrals: the difference of these energies yields the ionization energy of the neutral. In spectroscopy, ionization potentials are measured by removing an electron (usually by a laser beam or a He lamp) from the neutral molecule and recording the kinetic energy of the ejected electrons. Since the starting geometry of the cation is the

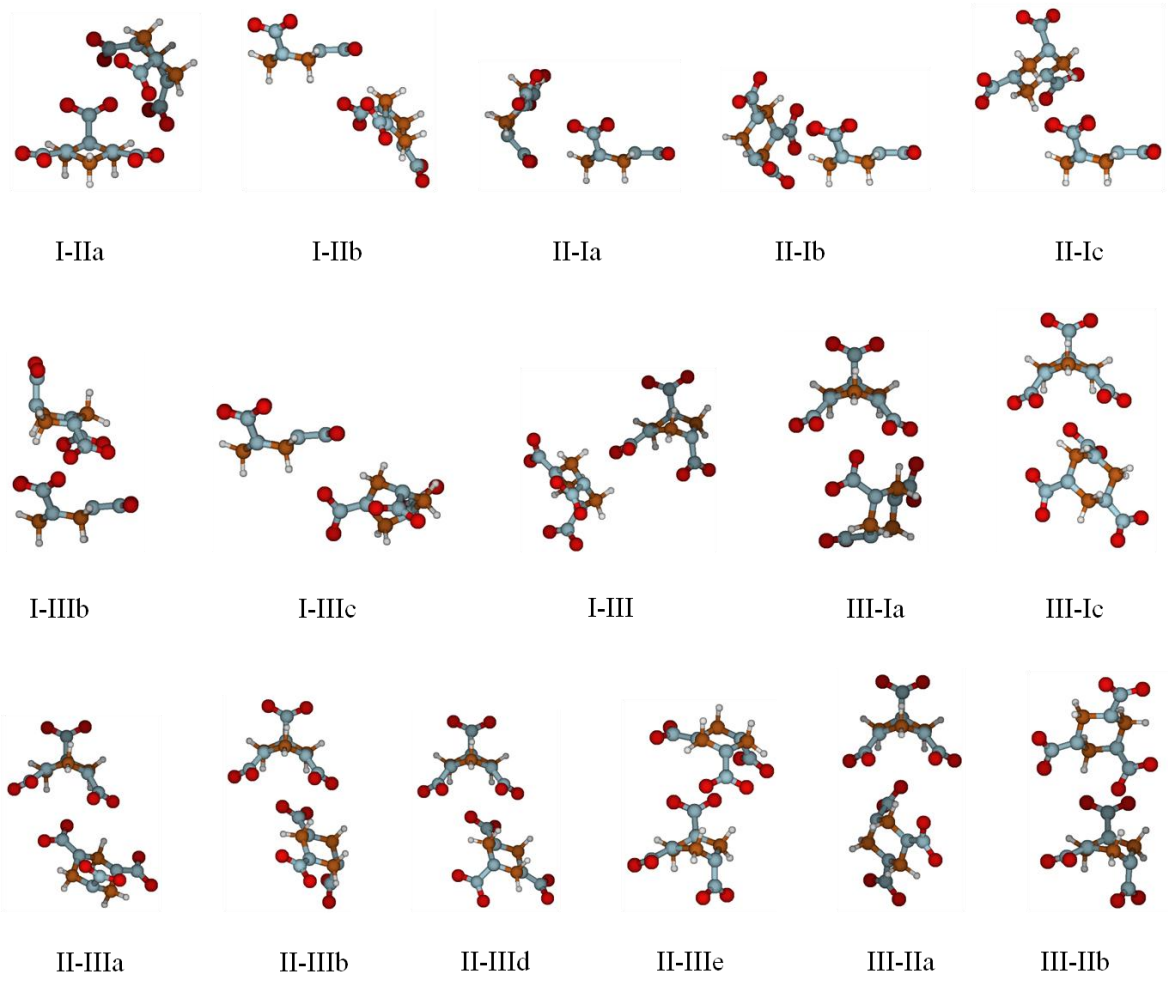

Figure 5.1. Optimized geometries of neutral $C_3H_6N_6O_6$ dimers (cont.).

same as that of the neutral in the experiments, we adopted a similar methodology in calculation of the cation structures. We removed an electron from the neutral and let the optimization proceed.

It is not certain that one will actually observe the rearrangements that occur during optimization in real experiments, since the coordinate step sizes used in optimization and those that occur in reality will be different. For example, in reality, once the cation structure drops into a potential energy well, no matter how shallow, it may not have enough energy to overcome it and may get stuck in a high energy local minimum. The calculation, if the default step size for the calculation is large enough, may explore other spaces on the potential energy surface and drop the cation into a deeper well. The structural changes observed, no matter how far-fetched they may be in the absence of any spectroscopic data, provide a set of possibilities that are worth reporting.

Table 5.1. Bond lengths in each type of monomer with their minimum and maximum values in neutral dimers. All bond lengths are in Angstrom.

	1st MONOMER				2nd MONOMER			
Dimers	N-N	N-O	C-N	C-H	N-N	N-O	C-N	C-H
I-I4	1.398-1.43	1.219-1.232	1.450-1.475	1.084-1.10	1.389-1.426	1.223-1.232	1.45-1.479	1.084-1.098
I-Ik	1.401-1.430	1.222-1.228	1.452-1.475	1.084-1.089	1.401-1.43	1.222-1.228	1.452-1.476	1.084-1.099
I-I7	1.397-1.428	1.222-1.230	1.449-1.476	1.084-1.10	1.40-1.43	1.221-1.228	1.448-1.477	1.084-1.10
I-I8	1.399-1.427	1.223-1.230	1.448-1.477	1.084-1.099	1.401-1.421	1.223-1.227	1.451-1.477	1.084-1.099
II-IIa	1.377-1.436	1.221-1.238	1.448-1.48	1.084-1.101	1.376-1.436	1.221-1.237	1.449-1.48	1.084-1.102
II-IIc	1.396-1.416	1.224-1.229	1.456-1.468	1.084-1.103	1.387-1.435	1.221-1.232	1.450-1.477	1.084-1.102
II-IIq	1.394-1.441	1.220-1.231	1.450-1.474	1.084-1.104	1.399-1.436	1.222-1.228	1.453-1.473	1.084-1.104
II-II4 (V-II)	1.412-1.421	1.221-1.23	1.461-1.466	1.084-1.094	1.394-1.432	1.222-1.230	1.451-1.476	1.084-1.099
II-II5	1.391-1.437	1.22-1.233	1.449-1.475	1.085-1.104	1.397-1.432	1.222-1.228	1.452-1.476	1.084-1.104
II-IIv	1.399-1.423	1.222-1.228	1.45-1.474	1.084-1.104	1.394-1.424	1.223-1.229	1.452-1.471	1.084-1.104
II-II2z	1.395-1.433	1.222-1.229	1.451-1.476	1.084-1.101	1.404-1.415	1.225-1.227	1.455-1.471	1.084-1.104
II-IIw (I-II)	1.403-1.423	1.222-1.23	1.452-1.477	1.084-1.099	1.383-1.433	1.222-1.234	1.450-1.477	1.084-1.101
III-III1	1.387-1.424	1.228-1.232	1.451-1.486	1.085-1.096	1.382-1.426	1.223-1.238	1.449-1.483	1.085-1.093

Table 5.1. Bond lengths in each type of monomer with their minimum and maximum values in neutral dimers. All bond lengths are in Angstrom (cont.).

	1st MONOMER				2nd MONOMER			
Dimers	N-N	N-O	C-N	C-H	N-N	N-O	C-N	C-H
III-III3 (IV-III)	1.37-1.425	1.223-1.238	1.448-1.49	1.087-1.093	1.383-1.423	1.224-1.237	1.453-1.489	1.085-1.096
III-III4	1.382-1.425	1.223-1.233	1.453-1.487	1.085-1.096	1.385-1.423	1.224-1.239	1.452-1.489	1.086-1.096
III-III7 (IV-IV)	1.370-1.426	1.222-1.236	1.450-1.487	1.088-1.095	1.372-1.424	1.223-1.243	1.449-1.489	1.087-1.093
III-III9 (IV-IV)	1.369-1.425	1.223-1.239	1.449-1.491	1.087-1.093	1.369-1.425	1.223-1.239	1.449-1.492	1.087-1.093
I-IIa (V-II)	1.401-1.418	1.222-1.229	1.458-1.463	1.086-1.095	1.398-1.425	1.218-1.228	1.451-1.474	1.084-1.104
I-IIb	1.385-1.426	1.222-1.233	1.45-1.479	1.084-1.097	1.398-1.415	1.221-1.23	1.453-1.475	1.084-1.104
II-Ia	1.393-1.423	1.221-1.229	1.453-1.47	1.084-1.104	1.40-1.428	1.222-1.228	1.450-1.477	1.084-1.099
II-Ib	1.395-1.422	1.224-1.23	1.452-1.47	1.084-1.104	1.40-1.428	1.222-1.228	1.449-1.477	1.084-1.099
II-Ic	1.394-1.433	1.222-1.229	1.451-1.476	1.084-1.101	1.403-1.433	1.221-1.229	1.403-1.433	1.084-1.099
I-IIIb (I-IV)	1.40-1.427	1.222-1.227	1.45-1.476	1.084-1.099	1.389-1.42	1.223-1231	1.451-1.48	1.086-1.096
I-IIIc	1.383-1.426	1.222-1.232	1.45-1.48	1.084-1.097	1.368-1.417	1.224-1.237	1.453-1.48	1.086-1.096
I-III	1.395-1.423	1.223-1.229	1.451-1.48	1.084-1.097	1.37-1.423	1.223-1.235	1.447-1.484	1.086-1.095
III-Ia (IV-I)	1.375-1.424	1.223-1.237	1.450-1.485	1.087-1.094	1.398-1.429	1.218-1.233	1.453-1.473	1.084-1.099

Table 5.1. Bond lengths in each type of monomer with their minimum and maximum values in neutral dimers. All bond lengths are in Angstrom (cont.).

	1st MONOMER				2nd MONOMER			
Dimers	N-N	N-O	C-N	C-H	N-N	N-O	C-N	C-H
III-Ic (IV-I)	1.375-1.425	1.223-1.234	1.449-1.489	1.087-1.093	1.384-1.435	1.221-1.236	1.384-1.435	1.084-1.10
II-IIIa (II-IV)	1.38-1.44	1.22-1.239	1.448-1.474	1.084-1.103	1.384-1.424	1.223-1.235	1.452-1.485	1.086-1.094
II-IIIb (II-IV)	1.375-1.436	1.221-1.237	1.453-1.481	1.084-1.101	1.369-1.425	1.223-1.24	1.448-1.49	1.087-1.093
II-IIId (II-IV)	1.375-1.437	1.221-1.238	1.449-1.481	1.084-1.102	1.37-1.425	1.223-1.239	1.448-1.491	1.087-1.093
II-IIIe (I-III)	1.397-1.426	1.22-1.23	1.451-1.474	1.084-1.10	1.387-1.421	1.225-1.232	1.451-1.485	1.086-1.092
III-IIa (IV-II)	1..378-1.424	1.223-1.34	1.449-1.487	1.087-1.093	1.40-1.408	1.223-1.23	1.451-1.474	1.084-1.104
III-IIb	1.386-1.425	1.223-1.31	1.453-1.486	1.086-1.096	1.40-1.415	1.221-1.227	1.453-1.474	1.084-1.104

With a data set of 33 neutrals belonging to a common symmetry group of C_1, it is also possible to build statistics of these possibilities of "structural change" and the resulting ionization potentials. Therefore this study does not aim to build a one-to-one relationship between neutral-cation pairs involved in the ionization process. Rather, separate pools of neutrals and cations are produced. In principle, any of the neutrals could become any of the cations. The structural changes that came about as a consequence of optimization provide the points on potential energy surfaces which could be studied in a more controlled fashion in a future study.

The cation complex structures are shown in Figure 5.2. During optimization, the neutral II-Ia and II-Ib complexes converged to the same cation as that of II-IIv, II-Ic neutral complex converged to the II-IIw cation, and the III-III1 neutral complex converged to the III-III3 cation. The II-II4 and II-II5 complexes optimized to a transition state which

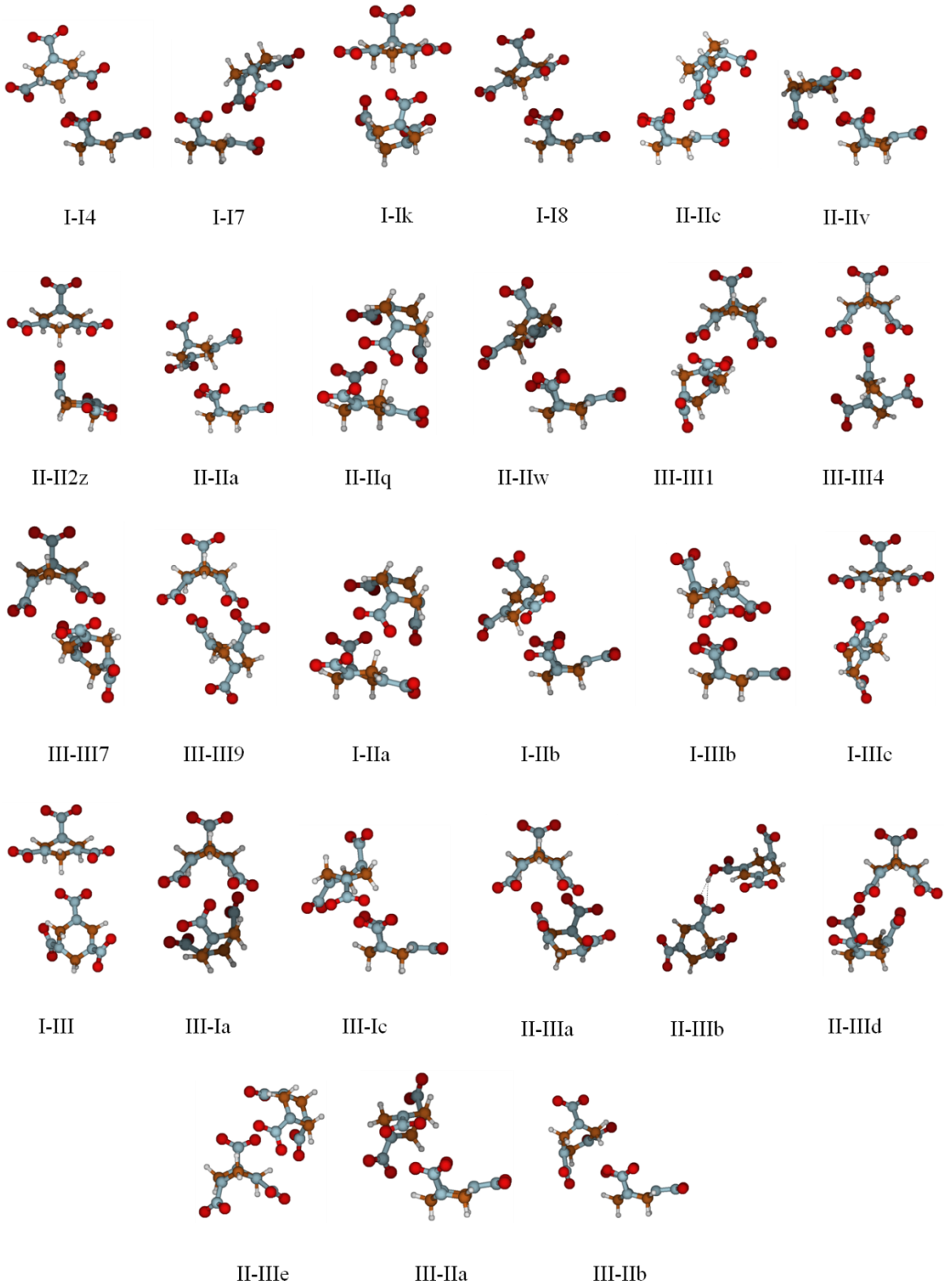

Figure 5. 2. Optimized geometries of cation dimers of $C_3H_6N_6O_6$.

they could not overcome. As a result, the number of cations is 27 whereas the number of neutrals is 33 in this study.

Ionization of the 33 neutrals resulted in drastic rearrangements in the neutral structures. For this reason, only 9 complexes could preserve their isomeric composition after ionization and optimization. In 13 complexes (I-I4, I-I8, I-Ik, II-IIa, II-II2z, II-IIv, II-IIq, II-IIw, I-IIb, I-III, I-IIa, I-IIIc, II-IIIb) the C-H bonds were elongated, giving way to new $C^{-\delta}\cdots H^{+}\cdots{}^{-\delta}ON$ interactions. The C-H and H-O distances are shown in Table 5.2. The C-H bond length in the neutral dimers were of 1.1Å at their longest. In Table 5.2, the bond lengths start from 1.152 Å at II-IIa cation. Structure of II-IIw, which is an average case, is chosen as an example and is shown in Figure 5.3.

Table 5.2. The $C^{-\delta}\cdots H^{+}\cdots{}^{-\delta}ON$ bond lengths in the proton-bound cationic dimers. All bond lengths are in Angstroms.

Cation	**$C^{-\delta}\cdots H^{+}$ distances (Å)**	**$H^{+}\cdots{}^{-\delta}ON$ distances (Å)**
II-IIa	1.152	1.824
I-I8	1.169	1.699
II-II2z	1.171	1.709
II-IIw (II-Ic), I-IIb	1.180	1.647
I-Ik	1.183	1.633
I-I4	1.203	1.559
I-III	1.217	1.529
II-Ia (II-Ib, II-IIv, I-IIa), II-IIq	1.217	1.521
I-IIIc	1.231	1.492

In one of these complexes (II-IIIb, shown in Figure 5.4), after transferring from isomer III to the (O)NO group of isomer II forming an –(HO)NO functionality, the proton became part of a hydrogen bond between the -(HO)NO of isomer II and the (O)NO group of isomer III. The $O^{-\delta}\cdots H^{+}$ distance ($(ON)O^{-\delta}\cdots H(ONO)$) is 1.673 Å and the H-O(NO) bond is 1.000 Å. The N-N bond between the ring and the nitrogen of the –(HO)NO functionality elongated to 1.48 Å. Experimental studies of the HONO molecule yielded r_{OH} of 0.954 Å, $r_{ON(O)}$ of 1.433 Å, r_{NO} of 1.177Å, a_{HON} of 102.1°, and a_{ONO} of 110.7°. In our calculations the HONO moiety formed on the isomer II gives r_{OH} of 1.005 Å, $r_{ON(O)}$ of 1.386 Å, r_{NO} of 1.235 Å, a_{HON} of 105.0°, and a_{ONO} of 121.1°. The d_{HONO} is 101.7°.

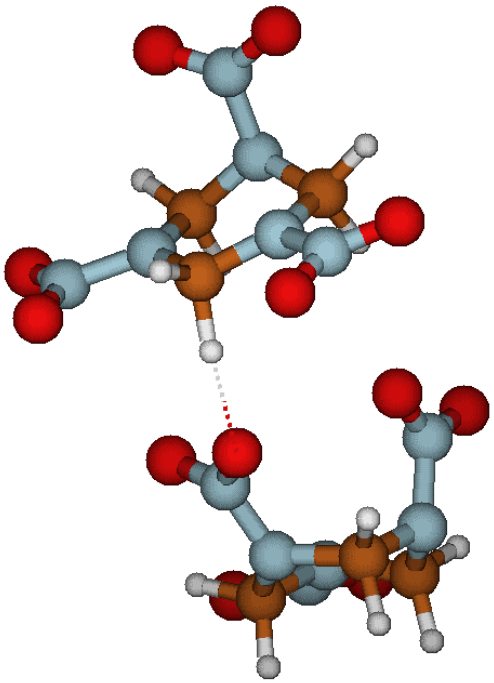

Figure 5.3. The B3LYP/6-31+G(d,p) geometry of the II-IIw cation. The dotted line indicates the new O-H interaction.

The calculated a_{ONO} values for the other $–NO_2$ substituents at this level are in the 125-130° range. The calculated a_{ONO} value for free $–NO_2$ is 134°. Therefore it is possible that this structure of II-IIIb corresponds to an early stage in the formation of HONO, where the a_{ONO} is half-way between that of HONO and $–NO_2$, and the d_{HONO} is half-way between that of *trans*-HONO (180°) and *cis*-HONO (0°). It appears that the presence of another monomer nearby catalyzes HONO formation.

The N-N bond lengths in 7 complexes, namely, I-I7, III-III3, III-III7, III-III9, II-IIIa, and II-IIIe increased, putting a distance between the $-NO_2$ groups and the ring system. While the N-N bond lengths varied between 1.35 and 1.44 Å in the neutral and cationic complexes, in the cations mentioned above the N-N bond length exceeded 1.50 Å. It is important to note that the charge on the NO_2 group is zero in these cations. These are charge-dipole complexes between the NO_2 groups and the charge-bearing rest of the complex. With the exception of I-I7, all of the cations above had the charge on an isomer III or isomer IV and the NO_2 groups broke off of these isomers (III,III,IV,IV,IV, respectively). The I-I7 cation carries the charge on isomer I from which the NO_2 broke off.

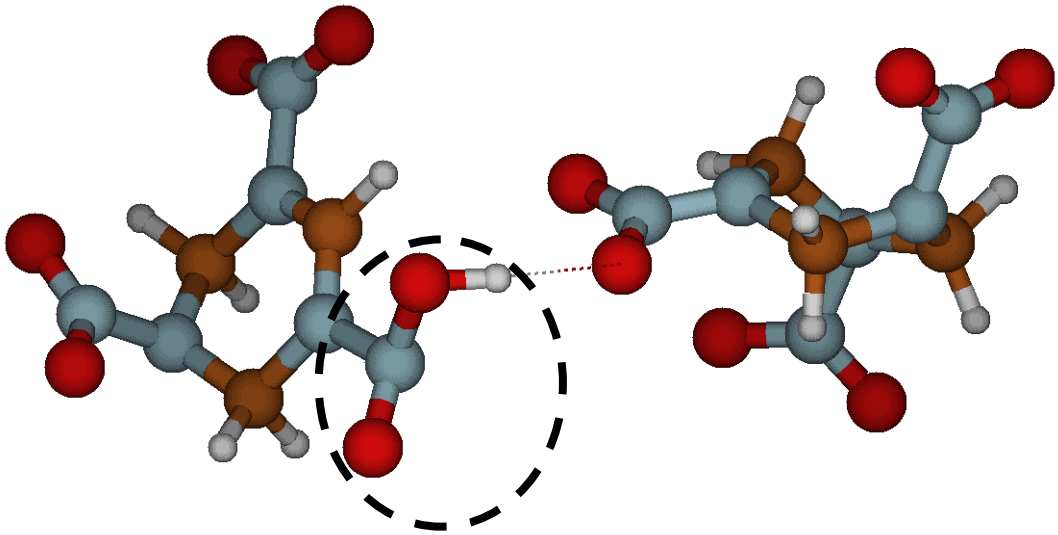

Figure 5.4. The B3LYP/6-31+G(d,p) geometry of the II-IIIb cation. The new HONO-like functionality is shown with a dashed circle.

The cations II-IIc, III-IIa, III-IIb, II-IIIb and II-IIId exhibited long N-N bonds between 1.48-1.49 Å however these lengths are below 1.50 Å.

The proton transfer complexes and the NO_2 charge-dipole complexes form different molecular sets; not one complex has gone through both processes during optimization. Only two of the nine cations that preserved their isomeric composition survived the structural rearrangements mentioned above.

In Figure 5.5 the population of isomers in the neutral and cation dimers are shown. The populations were calculated by counting the number of times a particular isomer was encountered in all the dimers. For instance, a I-I dimer provides a count of 2, a I-II dimer gives a count of 1 for isomer I. In neutral dimers, I and II are the most dominant isomers and isomer V is the least observed. Going from neutral to cationic dimers the most prominent change is observed in the population of isomer V. Ionization resulted in an increase in the percentage of isomer V in the complexes. Considering that isomers I and II are the two lowest energy isomers, their respective populations do not exceed 50% neither in the neutral set nor in the cation set. With the dimers that keep their isomeric content intact upon electron loss aside, despite the NO_2 liberation and $C^{-\delta}\cdots H^{+}\cdots{}^{-\delta}ON$ formation, the cationic monomers of the dimers stay within the set of I-V neutral set of conformations,

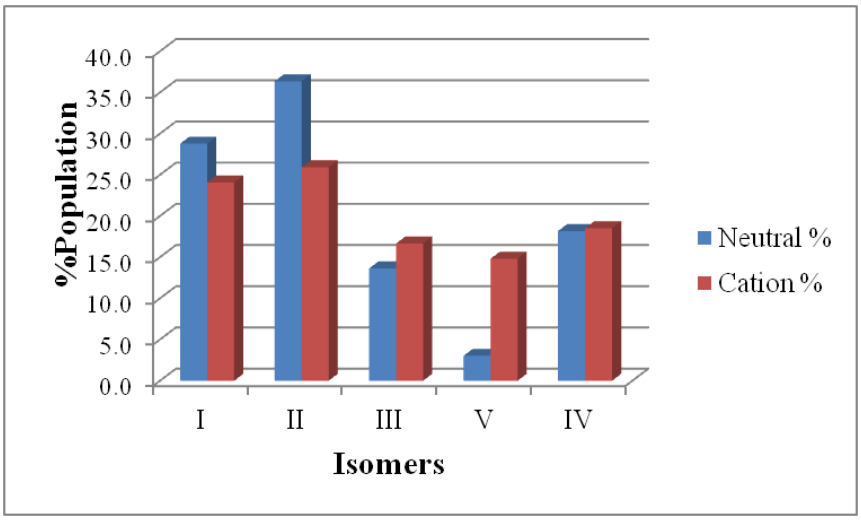

Figure 5.5. The isomeric populations of $(C_3H_6N_6O_6)_2$ and $((C_3H_6N_6O_6)_2)^+$ structures.

a new conformer VI or VII does not appear in all these dimers.

Ionization creates great strain in these complexes and more than 90% of the complexes relax by bond elongation and changing the position of the -NO_2 group with respect to the C-N-C-N-C-N ring (i.e. isomerizing). These results are in agreement with the results observed by mass spectrometry. Even though cluster/complex formation may be possible under vacuum and at cold cluster temperatures, the variety of ion processes following ionization, if the ionized complex is allowed enough time, are revealed in this study.

In Figure 5.6, plausible decomposition mechanisms of the $C_3H_6N_6O_6$ monomer are shown based on the fragments obtained from the mass spectrometry experiments. The mechanisms proposed, including N-N cleavage of the side N-NO_2 chains with subsequent C-N ring decomposition, ring C-N cleavage as the primary $C_3H_6N_6O_6$ thermal decomposition step and HONO elimination by atomic migration, have not been established by conclusive experimental evidence, but have been for the most part supported by theoretical studies. In the dimers of this study, while NO_2 expulsion happens independently on one monomer, the $C^{-\delta}\cdots H^{+}\cdots{}^{-\delta}ON$ formation happens between two monomers as a possible step for HONO formation. The energetic differences between intermolecular and intramolecular aspect of this reaction are part of our future studies.

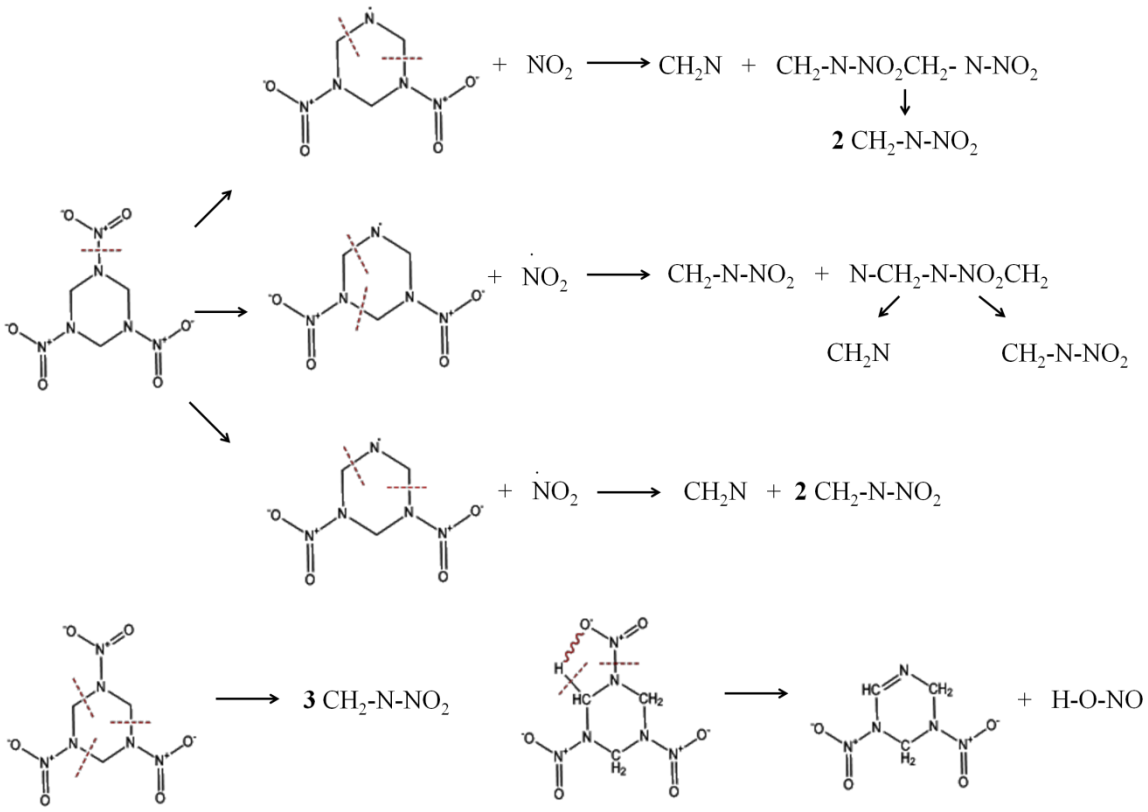

Figure 5.6. Plausible $C_3H_6N_6O_6$ decomposition mechanisms according to fragments obtained from mass spectrometry experiments done by Zhao *et al*.[27].

Extensive fragmentation of the dimers upon cationization threatens the detection of the parent ion of a dimer. The NO_2 expulsion occurs on a single monomer leaving the other intact, therefore it could be possible to detect $[C_3H_6N_6O_6]^+$. However the $C^{-\delta}\cdots H^+\cdots{}^{-\delta}ON$ formation occurs over both monomers, as a possible first step in production of HONO from the H of one monomer and the NO_2 of the other monomer.

As a preparation for calculating intermolecular potentials as a structural plausibility check, we calculated the center-of-mass distances between the neutral monomers in the neutral dimers, later to be increased and decreased to monitor the change in intermolecular potential. To calculate the center-of-mass of the dimers firstly cartesian coordinates of each atom in a monomer were multiplied with their atomic masses and were summed. The sum was divided by the molecular weight of the monomer. As a result, the Cartesian coordinate of a dummy atom which is located at the center of mass of the monomer was found. By

vectoral subtraction of the center of mass coordinates of two monomers their center of mass distances were calculated. In Figure 5.7 the center of mass distances of neutral and cation dimers are shown.

Among the neutrals, both I-IIa and I-IIIb dimers have the smallest mass center distances and the I-III dimer has the maximum center-of-mass distance. In cation dimers I-IIa again has the minimum center-of-mass distance however, II-IIIb has the maximum center of mass distance. There is an obvious decrease in the distances between monomers during ionization. This decrease stems from the stronger charge-dipole interaction in the cation dimers and more favorable positioning of monomers to avoid functional group repulsions. In the II-IIIb cation dimer the monomers appear further away from each other than in the neutral. A reaction has already occurred and produced a HONO-like moiety on one of the monomers making it bulkier and shifting its center-of-mass. Looking at center-of-mass differences alone could be misleading when cation longevity and detection are concerned. Even though II-IIIb cation seems to have the largest distance between the monomer mass centers, it is in fact 100 kJ/mol more stable than and is the most stable of all the cations found in this study.

5.2. Energetics

5.2.1. Relative Energies

The lowest energy neutral isomers are the most likely to survive and to yield cations in an ablation plume. Mass spectrometry does not distinguish between structural isomers unless the molecular ion is forced into a chemical process which distinguishes the isomerism based on stereoselectivity or spectroscopic properties in the gas phase prior to detection. It is therefore essential to calculate the energetic ordering of the neutral dimers and to observe the relationship between isomeric composition and overall energetics. Equally important is the knowledge on higher energy species since the beginnings of plume formation are far from thermodynamic equilibrium and higher energy dimers may be kinetically favored.

When the cations are considered as a dimer set independent of the neutrals they originate from, their energetic ordering reflects their stability and could correlate with their

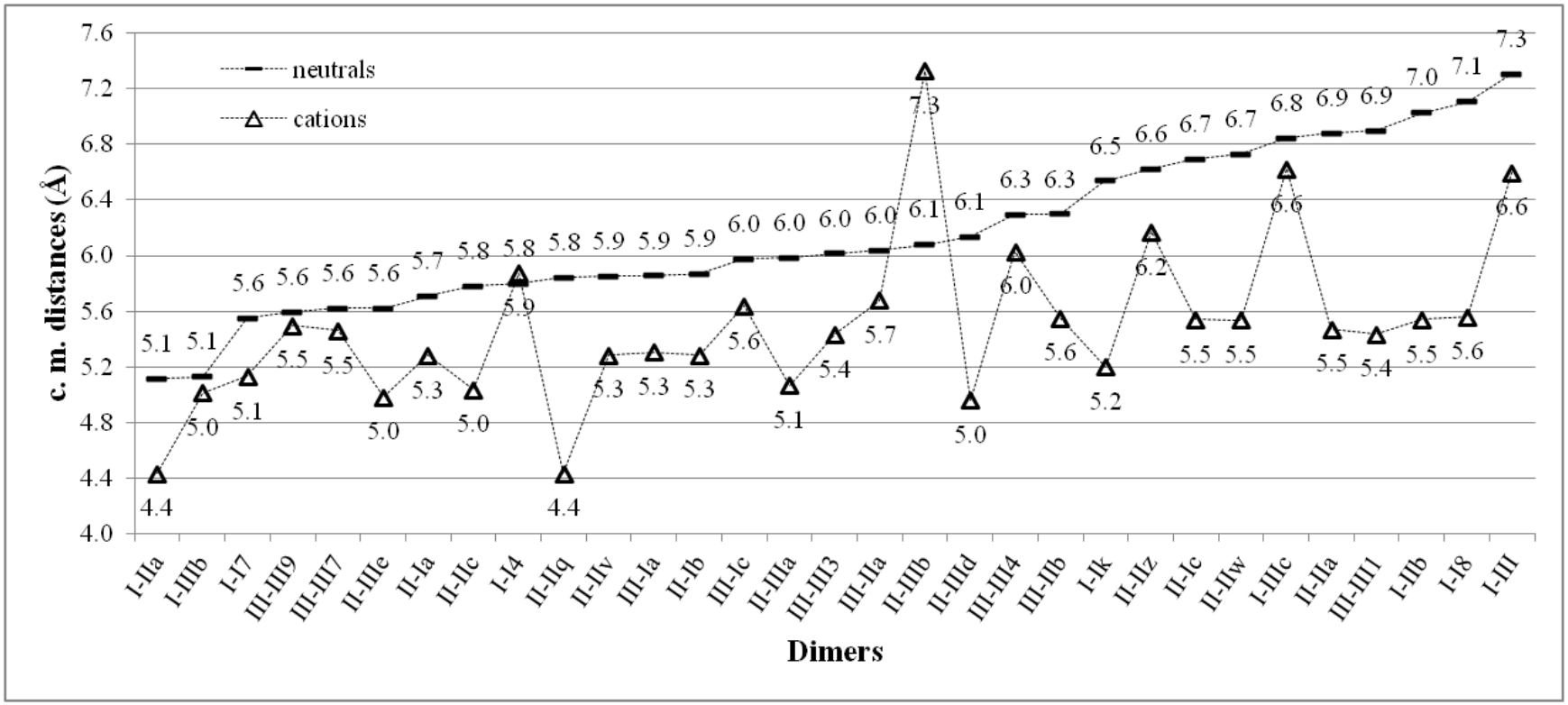

Figure 5.7. Center of mass distances of neutral and cationic dimers.

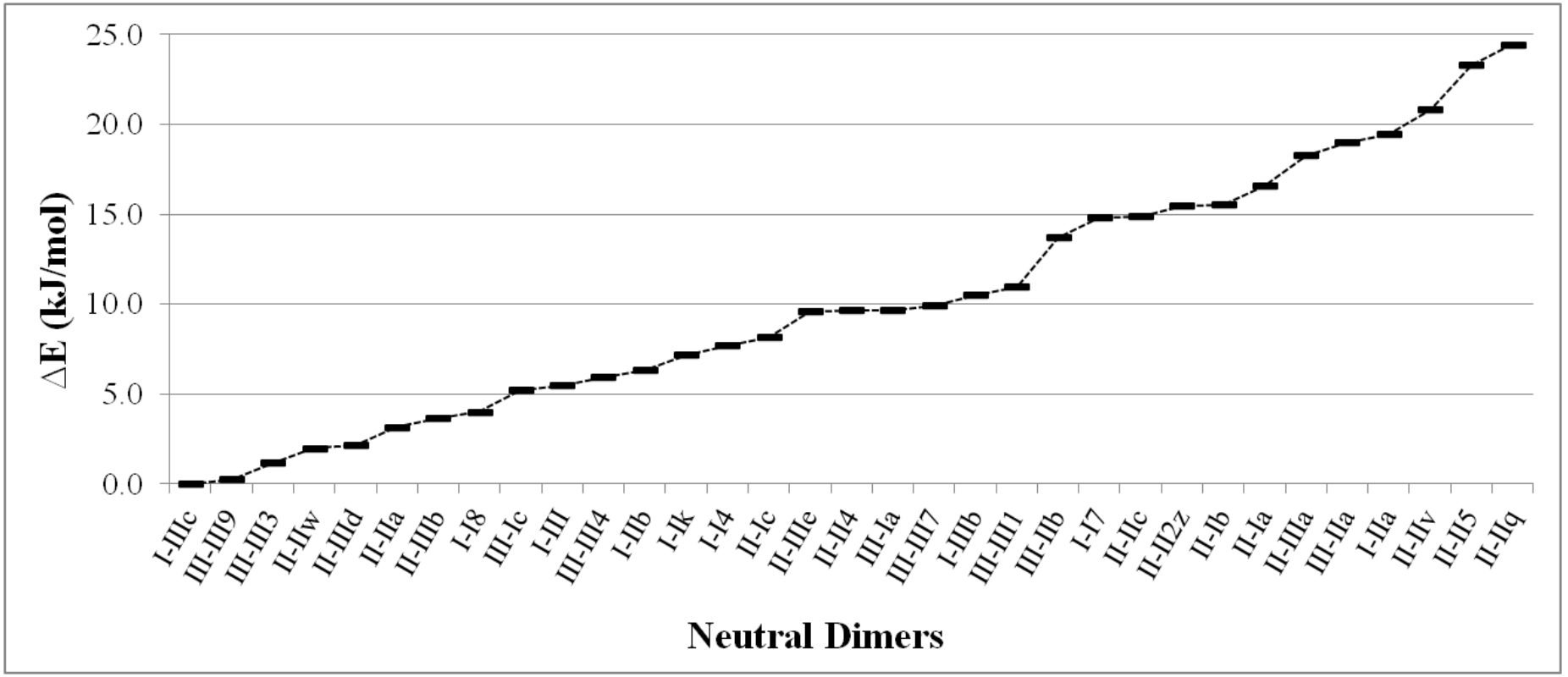

Figure 5.8. Relative energies of neutral dimers.

detectability. Their detectability ultimately depends on their unimolecular reactivity and timescale of their dissociation which are beyond the scope of this study. However, this study can reveal whether an energetically stable neutral gives rise to a less stable cation on the cation energy scale. Such a situation would lower the chances of detection of the neutral.

In Figure 5.8, the relative energies of neutral dimers with respect to the lowest energy dimer I-IIIc are shown. These energies were calculated using BSSE and zero-point corrected electronic energies of the neutral dimers. The energies are presented in Table 5.2. A more detailed account of the need for BSSE correction will be provided in the discussion concerning complexation energies.

The 33 neutral dimers are found to be in a 25 kJ/mol (6 kcal/mol) energy span. The energy curve forms plateaus as it rises. The I-IIIc, III-III9, III-III3, II-IIw, and II-IIId are the first five minimum energy neutral dimers in the set. In Figure 5.9, the isomeric composition is plotted against the energy. In Figure 5.10, the number of dimers within 5 kJ/mol intervals are shown.

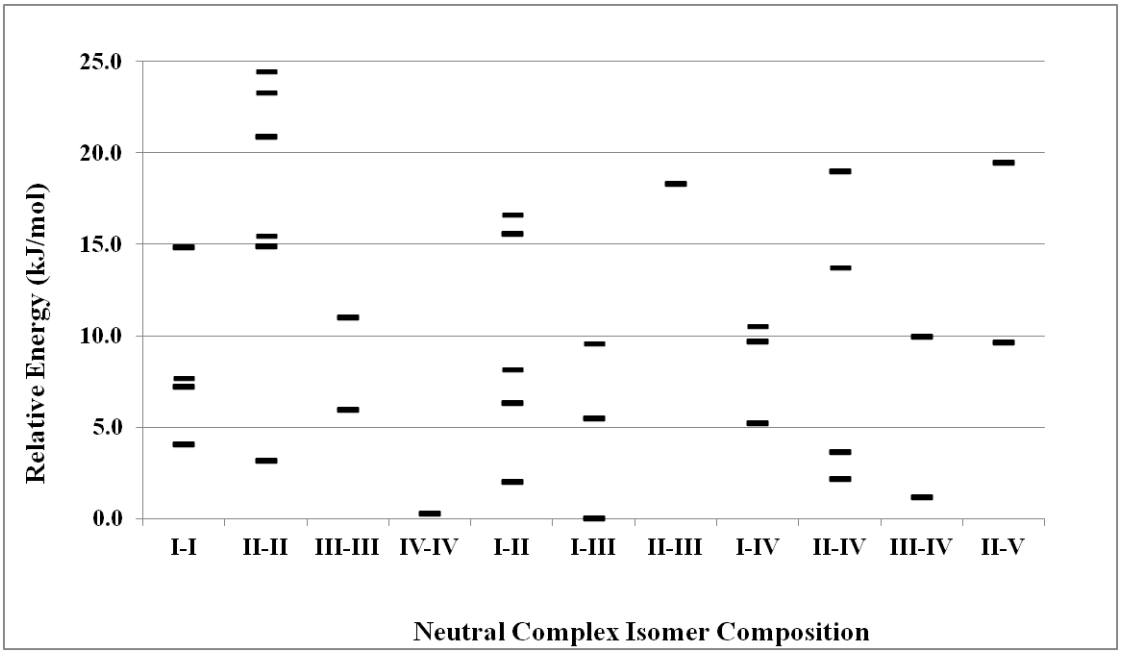

Figure 5.9. Variation in the neutral dimer isomeric composition on the relative energy scale.

In Figure 5.9, each column represents a set of rotational isomers. For instance, each bar in the I-I column is a rotational isomer where both monomers are I. Monomers I and II are the lowest energy monomers. Concurrently, they have the highest number of rotational isomers in the set, there are 6 of II-II, 5 of I-II, and 4 of I-I and II-IV (each) rotational isomers. However, especially in the case of II-II, all but one dimer are above 15 kJ/mol of relative energy.

According to Figure 5.9, with the exception of one dimer (II-IIa), rotational isomers of the II-II combination are all accumulated in the 15-25 kJ/mol interval. The 0-5 kJ/mol interval is highly populated by dimers having isomer IV. The energy ordering calculated by the B3LYP/6-31+G(d,p) method is I < II< III< V< IV. This ordering does not change when calculated by the B3LYP/Aug-cc-pVTZ method. One would expect a similar ordering with the dimers; those containing I would be expected to be the lowest energy dimers. However, the lowest energy structures are attained when the highest energy isomer III transforms into an even higher energy isomer (IV or V) during optimization. The III-III9 dimer was stabilized by such a transformation of both of the monomers (III) and the III-III3 dimer was stabilized by the transformation of one of the monomers.

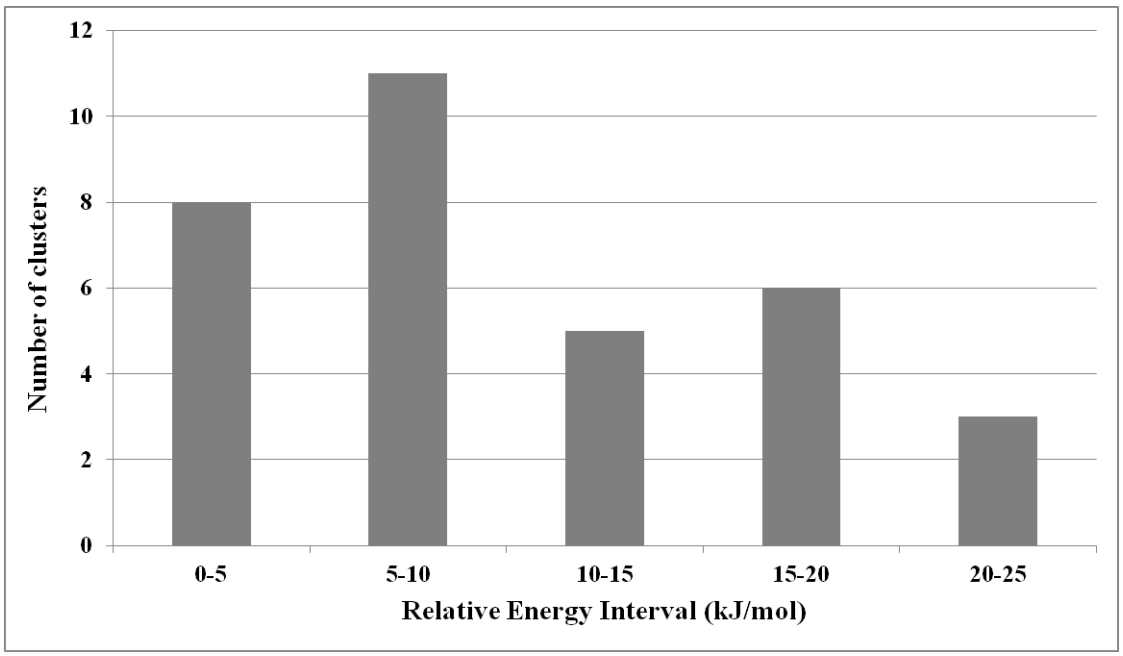

Figure 5.10. Number of neutral clusters per relative energy interval are shown.

These observations attest to the fact that the interactions between monomers, rather than their individual energetic stability, determine the overall energetics of the dimers. Locating a global minimum takes no less effort than inclusion of all known isomers into the pool and have them mix and stabilize with each other. We started with only three (I, II, III) of the five isomers to construct the dimers. It could be possible that the 0-5 kJ/mol interval could be more populated had we also included IV and V. This could explain lack of more IV-IV rotational isomers.

5.2.2. Complexation Energies

The isomerization of the monomer occurs through two major motions. One of them is the bending of the $(N\text{-}C\text{-}N)_{ring}$-N(O)(O) dihedral. This changes the orientation of the $-NO_2$ group with respect to the heterocyclic C-N-C-N-C-N ring. The ring system assumes boat and chair positions and this is the second motion leading to isomerization. The molecular orbital distributions and the charge distributions could illuminate the mode of interactions between monomers. However, before going into detail about interactions one more energetic parameter should be considered. This parameter is the complexation energy which is also called binding energy or loosely, dissociation energy in the literature. It is calculated by subtracting the zero-point corrected electronic energies of the monomers from that of the dimer they form. They are shown in Table 5.3.

All calculated complexation energies are negative and all complex formation reactions are exothermic. Only the complexes whose formation is more exothermic than -23 kJ/mol could exist *definitely*. These complexes are I-IIIc, III-III9, III-III3, II-IIId, II-IIIb, II-IIa, III-Ic, III-III7, II-IIw, III-III4, I-IIIb, III-IIa, II-II4, and III-Ia. According to the relative energies, the dimers that are most likely to be observed in the gas-phase are I-IIIc and III-III9 since a 0.3 kJ/mol energy difference is too small to eliminate III-III9 out of the picture**.**

The value of -23 kJ/mol is the vector sum uncertainty calculated using the mean absolute deviation (MAD) of the B3LYP/6-31+G(d,p) method (16 kJ/mol). Statistically, the complexation energies more positive than -23 kJ should be considered as uncertain. Basis set superposition error (BSSE) should also be considered as a factor that lowers the

Table 5.3. The energies of the $C_3H_6N_6O_6$ dimers computed at B3LYP/6-31+G(d,p) level are shown. Relative energies shown in the second column are calculated relative to the I-IIIc complex which has the lowest E+ZPE energy. See text for details on calculation of the complexation energy (BSSE corrected).

Name of dimers	E+ZPE (hartrees)	E+ZPE (rel,kJ/mol)	Complexation Energies (kJ/mol)
I-IIIc	-1794.632029	0.0	-21.6±23
III-III9	-1794.631928	0.3	-30.6±23
III-III3	-1794.631588	1.2	-26.5±23
II-IIw	-1794.631271	2.0	-20.3±23
II-IIId	-1794.631205	2.2	-26.2±23
II-IIa	-1794.630823	3.2	-22.7±23
II-IIIb	-1794.630643	3.6	-24.8±23
I-I8	-1794.630500	4.0	-14.7±23
III-Ic	-1794.630046	5.2	-19.6±23
I-III	-1794.629941	5.5	-16.1±23
III-III4	-1794.629775	5.9	-18.6±23
I-IIb	-1794.629620	6.3	-16.0±23
I-Ik	-1794.629288	7.2	-11.6±23
I-I4	-1794.629099	7.7	-11.1±23
II-Ic	-1794.628923	8.2	-16.7±23
II-IIIe	-1794.628379	9.6	-12.0±23
II-II4	-1794.628359	9.6	-16.9±23
III-Ia	-1794.628356	9.6	-12.0±23
III-III7	-1794.628252	9.9	-17.8±23
I-IIIb	-1794.628020	10.5	-14.3±23
III-III1	-1794.627851	11.0	-13.5±23
III-IIb	-1794.626813	13.7	-14.7±23
I-I7	-1794.626383	14.8	-3.9±23
II-IIc	-1794.626362	14.9	-11.0±23
II-II2z	-1794.626145	15.4	-10.5±23
II-Ib	-1794.626105	15.6	-6.8±23
II-Ia	-1794.625716	16.6	-5.7±23
II-IIIa	-1794.625062	18.3	-6.9±23
III-IIa	-1794.624796	19.0	-9.4±23
I-IIa	-1794.624618	19.5	-7.1±23
II-IIv	-1794.624090	20.8	-5.1±23
II-II5	-1794.623160	23.3	-2.6±23
II-IIq	-1794.622719	24.4	-1.5±23

energy of the supermolecule (the complex) bringing isomers together and forming complexes with exothermicity less than 23 kJ/mol. The calculated neutral complexes are kept together by long-range polarization forces such as the dipole-dipole interaction therefore the BSSE is expected to play a prominent role. It is also possible that due to cancellation of errors, the complexation energies are exact, however, the BSSE can not be ignored or cancelled out. With merely -8 kJ/mol complexation energy, the complexes II-II5 and II-IIq are the most likely candidates for BSSE induced artificial complexation. Therefore we calculated the complexation energies for the 9 lowest energy complexes with the counterpoise BSSE correction and for the 2 highest energy complexes, II-IIq and II-II5. We compared the uncorrected B3LYP/6-31+G(d,p) results with the BSSE corrected results and also with those calculated using the B3LYP/Aug-cc-pVTZ//B3LYP/6-31+G(d,p) method where the geometries and the zero-point corrections calculated using the 6-31+G(d,p) basis set were used for single-point energy energy calculations using the bigger aug-cc-pVTZ basis set. The latter was not done for II-IIq and II-II5. The complexation energies and the magnitude of the BSSE corrections for each complex are shown in Table 5.4.

Table 5.4. Energetics of $C_3H_6N_6O_6$ dimers which are computed at B3LYP/6-31+G(d,p) level are shown. Relative energies displayed in the second column are calculated relative to the I-IIIc complex which has the lowest E+ZPE energy. See text for details on calculation of the complexation energy.

	Complexation Energies (kJ/mol)			**BSSE Corrections (kJ/mol)**
Dimer	***B3LYP/ 6-31+G(d,p)***	***B3LYP/6-31+G(d,p) (BSSE corrected)***	***B3LYP/Aug-cc-pVTZ// B3LYP/ 6-31+G(d,p)***	
III-III9	-41.5	-30.6	-28.9	10.8
III-III3	-36.3	-26.5	-25.5	9.8
II-IIId	-35.4	-26.2	-25.2	9.2
I-IIIc	-27.7	-21.6	-21.2	6.1
II-IIIb	-33.9	-24.8	-23.9	9.1
III-Ic	-29.6	-19.6	-19.7	10.0
II-IIa	-29.7	-22.7	-22.5	7.0
III-III4	-26.3	-18.6	-18.1	7.7
I-I4	-19.8	-11.1	-12.6	8.7
II-IIq	-8.8	-1.5	-	7.2
II-II5	-8.6	-2.6	-	6.2

Comparison of the complexation energies of II-IIq and II-IIa with the BSSE corrections shows that the BSSE should not be overlooked. The magnitude of the BSSE (7.2, 6.2 kJ/mol) and the uncorrected 6-31+G(d,p) complexation energies (-8.8, -8.6 kJ/mol) are almost equal indicating that the two isomer II molecules in II-IIq and II-IIa came together artificially. After the BSSE correction the two highest energy complexes appear to be held together merely by less than 3 kJ/mol energy.

There is no apparent correlation between the magnitudes of the complexation energies and the BSSE. All complexes with BSSE of 9 kJ/mol and above (III-III9, III-III3, II-IIId, II-IIIb, III-Ic, III-III4) have isomers III and IV in their make-up. As the complexation energy becomes smaller and the isomers are more loosely bound to each other, the BSSE becomes significant relative to the complexation energy. Looking at the 11 lowest energy complexes, III-III9 has the largest BSSE in its complexation energy amounting to 10.8 kJ/mol. This is due to the fact that in the HOMO the electron resides on both IV isomers equally. However with a complexation energy of -30.6 kJ/mol this cluster can still claim its existence.

The BSSE corrected complexation energies calculated with the smaller 6-31+G(d,p) basis set approach the uncorrected values calculated using the aug-cc-pVTZ basis set. Using a larger basis set is expected to remove the deficiencies of the smaller basis set, making the BSSE insignificant. Looking at the BSSE corrected complexation energies (2nd column), based on the complexation energies alone, we can say III-III9, III-III3, II-IIId, and II-IIIb could exist in the gas phase. Experimental studies on anionic van der Waals clusters yielded a well-depth of 14.07±0.07 kJ/mol in $XeCl^-$ [68], 5.97 kJ/mol in ClD_2^- (*ortho*), 6.69 kJ/mol in ClD_2^- (*para*), and 5.84 kJ/mol in ClH_2^- [69]. Molecular systems closer to the size and constitution of $(C_3H_6N_6O_6)_2$ dimers, such as the neutral $(benzene)_2$, benzene-cyclohexane, $(toluene)_2$, benzene-toluene, $(para\text{-}difluorobenzene)_2$, and benzene-para-difluorobenzene clusters have dissociation energies of 6.8±1.0 kJ/mol, 7.7±1.9 kJ/mol, 14.5±1.0 kJ/mol, 12.5±1.0 kJ/mol, 8.7±1.9 kJ/mol, and 7.7±1.9 kJ/mol, respectively [70]. Benzene-water-methanol clusters were found to have binding energies around 100 kJ/mol [71], 544 cm^{-1} (6.5 kJ/mol) for S_0 Benzene·Acetylene (B·A), 1675 cm^{-1} (20.0 kJ/mol) > and 2380 cm^{-1} (28.5 kJ/mol) > for two isomeric $B{\cdot}A_2$ complexes [72]. Granted that the neutral clusters mentioned above have π-π stacking interactions as a

component of the dispersion interactions, even the benzene-cyclohexane complex was found to exist and have a finite well-depth. This is encouraging for the $(C_3H_6N_6O_6)_2$ dimers and their existence, however the complexation energies should be calculated by using a benchmark technique with known uncertainties.

Table 5.5. The BSSE corrected, uncorrected relative energies and the aug-cc-pVTZ energies.

	Relative Energies (kJ/mol)		
Complex	***B3LYP/ 6-31+G(d,p)***	***B3LYP/6-31+G(d,p) (BSSE corrected)***	***B3LYP/Aug-cc-pVTZ// B3LYP/ 6-31+G(d,p)***
III-III9	***0.0***	0.3	***0.0***
III-III3	1.9	1.2	1.7
II-IIId	3.5	2.2	1.6
I-IIIc	4.5	***0.0***	1.2
II-IIIb	5.1	3.6	3.0

In Table 5.5 the BSSE corrected and uncorrected relative energies of some complexes are given with 6-31+G(d,p) basis set and for comparison the energies that are calculated with the aug-cc-pVTZ basis set are also shown. The energy ordering between the BSSE corrected and uncorrected 6-31+G(d,p) sets and the aug-cc-pVTZ basis sets are different. The I-IIIc neutral dimer is the most stable dimer when the BSSE corrected energies are taken into account and it is the next most stable dimer when calculated with the aug-cc-pVTZ basis set. A handicap with the aug-cc-pVTZ calculation is that the 6-31+G(d,p) geometry may require small adjustments to reach the true aug-cc-pVTZ minimum. Since the energies are quite small, the basis set effect would be amplified. Therefore, out of the relative energies computed with the three methodologies above, the BSSE corrected energies should be preferred. When BSSE corrected energies are considered, III-III9, III-III3 and I-IIIc neutral dimers seem likely to form complexes in the plume at the room temperature, room temperature of 298 K corresponds to 2.5 kJ/mol and that would not be enough to form dimers from the minimum energy structure (I-IIIc) appearing at higher relative energies than 2.5 kJ/mol.

Combining the complexation energy and the relative energy information in Table 5.2, one can speculate that there are a minimum of 4 dimers (III-III9, III-III3, II-IIId, and I-IIIc) that can populate the neutral plume under thermodynamic conditions. The III-III9, III-III3, II-IIId are winners in both criteria (low relative energy and high complexation

energy). The I-IIIc wins on the relative energy front but loses in the complexation energy front however, since the uncertainty of 23 kJ/mol is no longer valid after the BSSE corrections, we made an exception for I-IIIc.

The zero-point corrected electronic energies of cation dimers relative to the II-IIIb cation dimer which has the minimum energy are plotted in Figure 5.11. Since the relative energies of first and second cation dimers are large, II-IIIb cation dimer was not shown in the plotted area. The II-IIIb cation is the lowest energy cation, more than 100 kJ/mol more stable than the next most stable cation. It is observed that the cations that go through proton transfer share a common structural motif, isomer II. It is the -N-CH_2-N- group which is on the symmetry plane of the isomer II that parts from its proton during the proton transfer.

5.2.3. Ionization Energies

The ionization energies are shown in Table 5.6. The uncertainty of the B3LYP/6-31+G(d,p) ionization energies is ±0.2 eV. In order to assess the ionization energy performance, we calculated the ionization potential of molecules that resemble $C_3H_6N_6O_6$. The experimental ionization energy for NO_2 is 9.586±0.002 eV [NIST Database Number 69]. The comparison is presented in Table 5.7. For NO_2 and NO_2-NO_2, the B3LYP/6-31+G(d,p) vertical and adiabatic ionization energies are within 0.5 eV of the experimental results. In the case of $(CH_3)_2$N-NO_2, which would provide the most suitable comparison, the cation optimized into a transition state, the energy difference yielded 9.4 eV. There was no experimental vertical ionization energy present in the literature for comparison. On these compounds, most of the HOMO electron density is on the –NO_2 groups the ionization energies of the complexes are close to each other because it takes similar amounts of energy to remove the electrons from similar HOMOs.

The ionization energy distribution per the number of complexes is shown in Figure 5.12. The average adiabatic and vertical ionization energies are 9.4 ve 9.8 eV, respectively. The neutral complexes are kept together by weak long-range polarization interactions. However among the cations there are those that experience charge-dipole interactions between the isomers, others which are proton-transfer complexes (between individual C-H and ON(O)- moieties) and a few charge-dipole complexes between the NO_2 groups and the

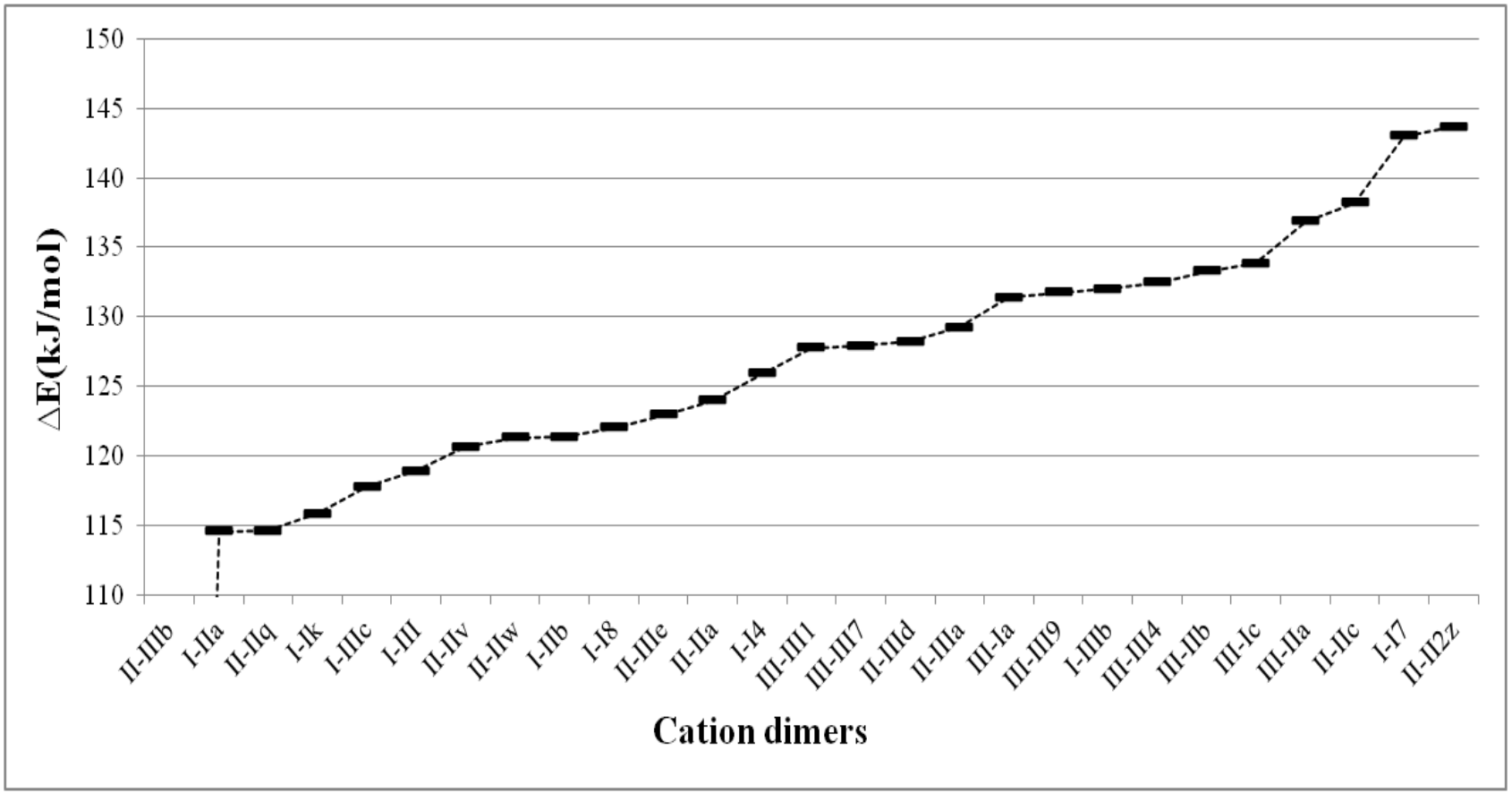

Figure 5.11. Relative energies of cation dimers. The lowest energy cation dimer is II-IIIb and is not shown on the ΔE scale for visibility purposes.

Table 5.6. The ionization energies of $[C_3H_6N_6O_6]_2$ computed at the B3LYP/6-31+G(d,p) level are shown. Relative energies are calculated with respect to dimer I-IIIc. The II-II4 and II-II5 neutrals did not converge to a minimum after ionization.

Name of the dimers	E+ZPE (rel,kJ/mol)	Ionization Energies (eV)	
		Vertical	Adiabatic
I	-	10.6±0.2	10.0±0.2
II	-	10.5±0.2	10.0±0.2
III	-	10.3±0.2	10.0±0.2
I-IIIc	0.0	9.9±0.2	9.4±0.2
III-III9	0.3	9.8±0.2	9.6±0.2
III-III3	1.2	9.8±0.2	9.5±0.2
II-IIw	2.0	9.8±0.2	9.4±0.2
II-IIId	2.2	9.9±0.2	9.5±0.2
II-IIa	3.2	10.1±0.2	9.4±0.2
II-IIIb	3.6	9.9±0.2	8.1±0.2
I-I8	4.0	9.8±0.2	9.4±0.2
III-Ic	5.2	9.8±0.2	9.5±0.2
I-III	5.5	9.8±0.2	9.3±0.2
III-III4	5.9	9.8±0.2	9.5±0.2
I-IIb	6.3	9.9±0.2	9.3±0.2
I-Ik	7.2	10.0±0.2	9.3±0.2
I-I4	7.7	9.7±0.2	9.4±0.2
II-Ic	8.2	9.9±0.2	9.3±0.2
II-IIIe	9.6	9.7±0.2	9.4±0.2
II-II4	9.6	9.7±0.2	-
III-Ia	9.6	9.7±0.2	9.4±0.2
III-III7	9.9	9.7±0.2	9.4±0.2
I-IIIb	10.5	9.7±0.2	9.5±0.2
III-III1	11.0	9.8±0.2	9.4±0.2
III-IIb	13.7	9.8±0.2	9.4±0.2
I-I7	14.8	9.7±0.2	9.5±0.2
II-IIc	14.9	9.8±0.2	9.4±0.2
II-II2z	15.4	9.8±0.2	9.5±0.2
II-Ib	15.6	9.8±0.2	9.2±0.2
II-Ia	16.6	9.7±0.2	9.2±0.2
II-IIIa	18.3	9.8±0.2	9.3±0.2
III-IIa	19.0	9.8±0.2	9.5±0.2
I-IIa	19.5	9.6±0.2	9.2±0.2
II-IIv	20.8	9.8±0.2	9.2±0.2
II-II5	23.3	9.9±0.2	-
II-IIq	24.4	9.9±0.2	9.1±0.2

Table 5.7. The experimental adiabatic and vertical ionization energies of molecules with similar HOMO structures.

Molecule	Adiabatic Ionization Energy (eV)		Vertical Ionization Energy (eV)	
	Experimental	***Calculated***	***Experimental***	***Calculated***
NO_2	9.586±0.002	10.1±0.2	11.23	11.9±0.2
NO_2-NO_2	10.8 ±0.2	10.3±0.2	11.4 ±0.1	11.6±0.2
$(CH_3)_2N$-NO_2	9.53	9.4±0.2	-	9.9±0.2

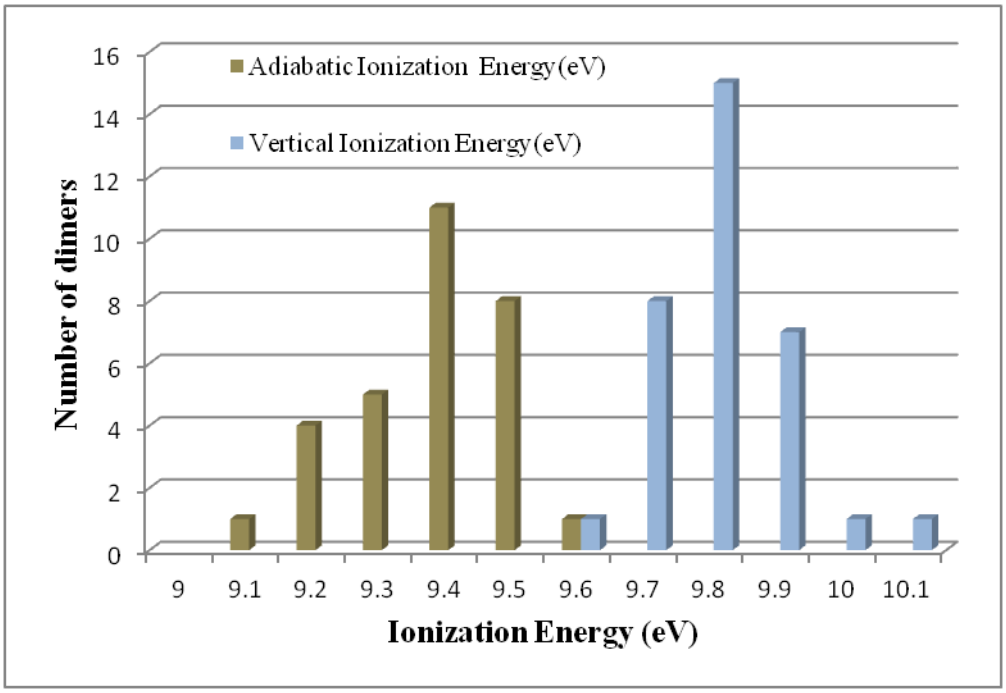

Figure 5.12. The distribution of Adiabatic and Vertical Ionization Energies of dimers.

cationic rest of the complex. Each of these factors result in different amounts of stabilization of the cation. Since the cation has a higher 0 K energy than its neutral, when it is stabilized, the ionization energy, which is the difference between the neutral and cationic states, is reduced. Therefore different amounts of stabilization leads to the distribution in the ionization energies.

The ionization energies of all the complexes are lower than the ionization energies of the individual isomers as in indicated as I, II and III in the first rows of the Table 5.6. The differences are within the limits determined by the method uncertainty, however.

With the exception of III-III9 and I-Ik complexes the electron is localized on one of the isomers in each neutral complex found in this study. We could therefore think of the homogeneous or heterogeneous neutral complexes as individual monomer solvated by similar or different monomers as in Monomer I· (Monomer II). The complexation energies calculated in this study define the energy of stabilization of one of the neutral monomers by the other. When the complexation energies reported in this work are converted to the eV scale in which the ionization energies were defined, they do not exceed 0.4 eV (based on the B3LYP/6-31+G(d,p) method). This is insignificant when the ionization energies of 9-10 eV are considered. For the complex ionization energy to be lower than that of the individual monomer, the cation monomer should be stabilized more than the neutral monomer by its solvent. Different than a single cationic monomer, the dimer cation enjoys stabilizing ion-dipole interactions with the solvent decreasing its energy furthermore, which would amount to more than 0.4 eV if 0.4 eV is the measure of dipole-dipole interaction energy for the particular complex.

Individual monomers and the dimers are different in that the monomers go through drastic ionization induced structural changes when solvated by another in the complex. In a way, presence of another monomer nearby catalyses bond breakage and in some cases formation of new bonds in the cationic state, lowering the energy difference between the neutral and the cation. Isomeric scrambling is another consequence of solvation. If the neutral isomeric composition is thought of as the "zero-state", the ionization induced isomeric scrambling towards creation of an isomeric pair that interacts energetically more favorably with each other is another big factor in reduction of the energy of cationic complex.

5.3. Molecular Orbitals and Charge Distributions

In Figure 5.13, the HOMO of the neutral $(C_3H_6N_6O_6)_2$ dimers are shown. An isosurface value of 0.08 has been used for visual construction. The complexes have been prepared by overlapping the HOMO of one with the LUMO of the other. The LUMO are located on the $–NO_2$ groups in the isomers I, II and III. The HOMO are located on the ring nitrogens and the ring $-CH_2$ also contributes.

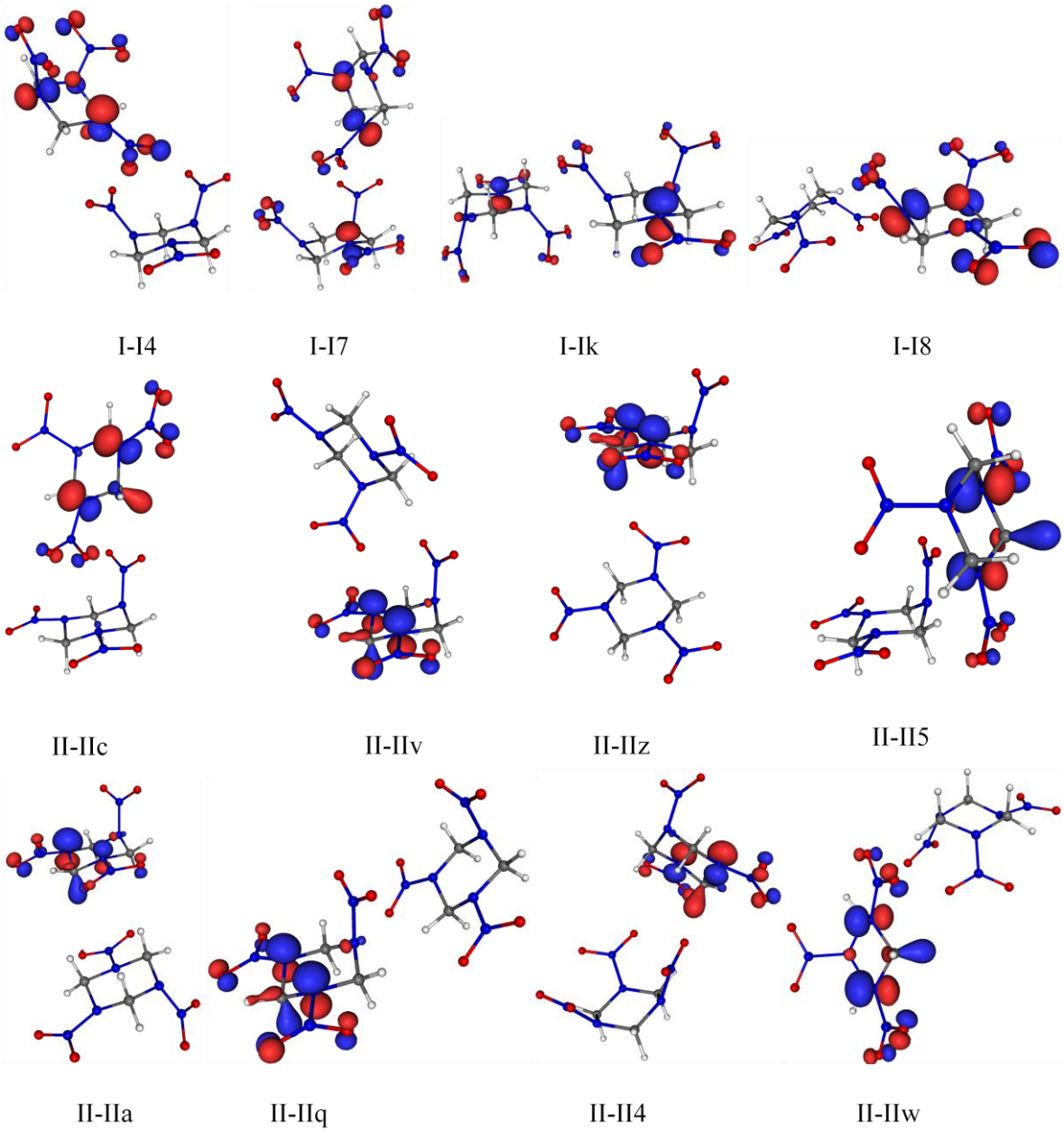

Figure 5.13. Representation of the HOMO and LUMO orbitals of $(C_3H_6N_6O_6)_2$ dimers.

All of the initial complex geometries where the isomers were brought together according to the HOMO-LUMO overlap went through changes during optimization. It is important to note that the HOMO energies of the 5 isomers making up the complexes were lower than all the LUMO energies. The 6-31+G(d,p) basis set results in orbitals with further spatial extent which obliges the isomers to move away from each other or to isomerize into others to reduce the intermolecular repulsive forces. The first observation is that the complex HOMOs are represented by the HOMOs of one or both isomers, no other

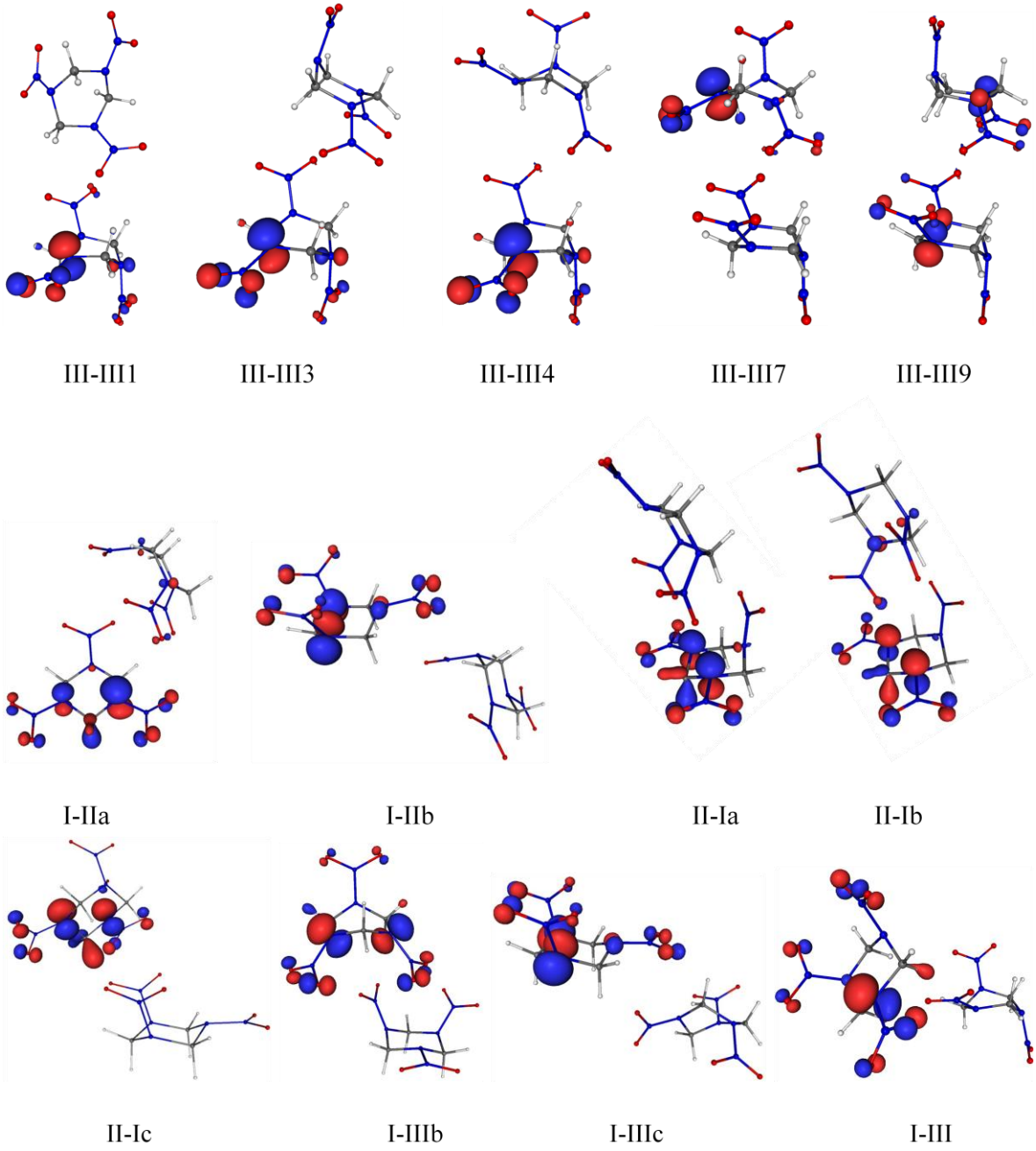

Figure 5.13. Representation of the HOMO and LUMO orbitals of $(C_3H_6N_6O_6)_2$ dimers (cont.).

The second observation is that only in the III-III9 and I-Ik complexes both isomers contribute substantially to the HOMO. In I-I7, I-IIa and II-Ib there is minor contribution from the p orbitals in the ring nitrogens and $–NO_2$ oxygens. The electron is on only one isomer in the other complexes. The ChelpG atomic charges per isomer within the complexes indicate that there is no substantial charge transfer between the isomers. As a result the complexes are kept together by weak polarization interactions.

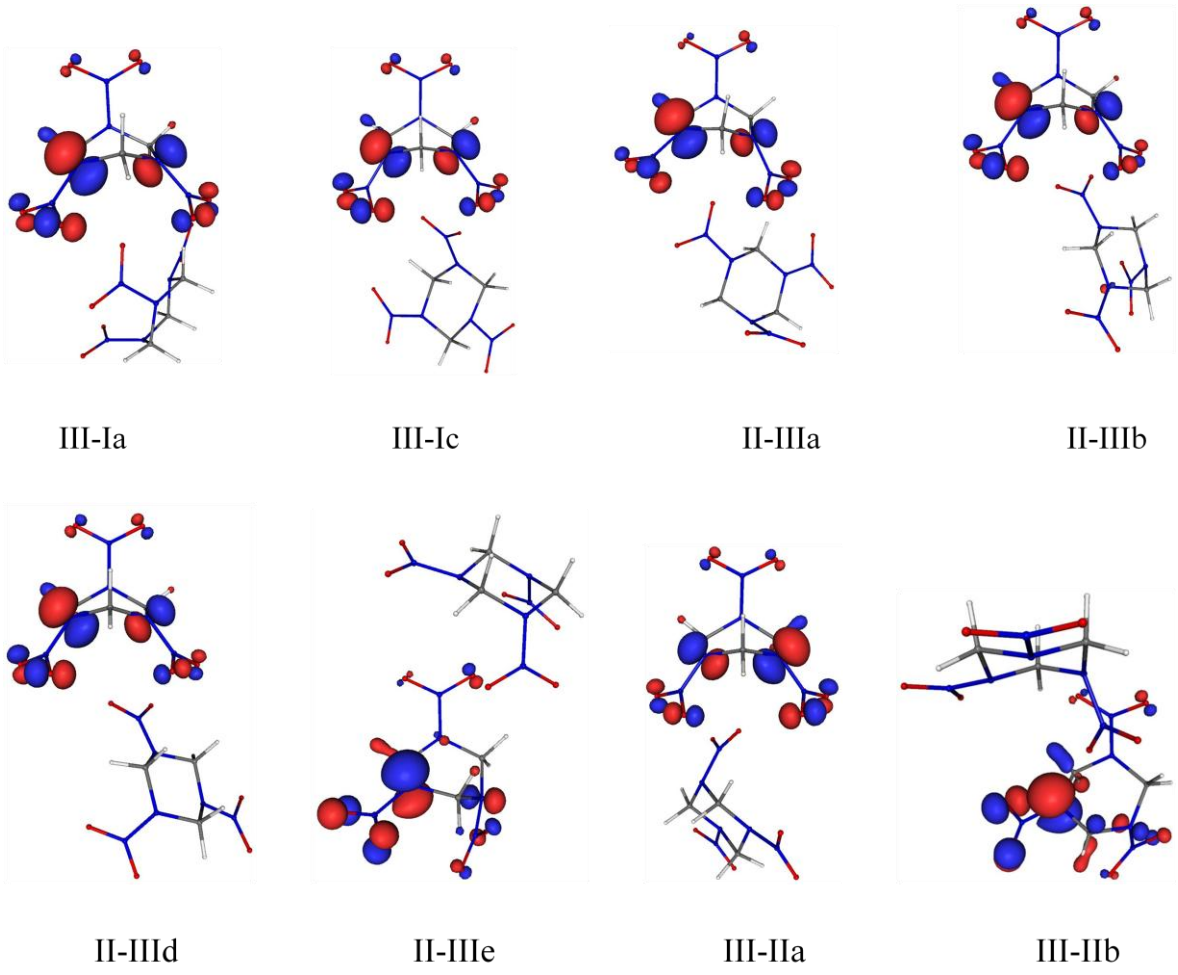

Figure 5.13. Representation of the HOMO and LUMO orbitals of $(C_3H_6N_6O_6)_2$ dimers (cont.).

Table 5.8 shows the location of HOMO orbitals in the neutral dimers on a monomer basis. In all the 8 neutral complexes with the II-II designation, I-III, I-IIa, II-1a, II-1b and II-1c the HOMO is localized on isomer II. In I-I4, I-I7, I-I8, I-Ik, I-IIb and I-IIIc the HOMO is on isomer I. In III-III9, I-IIIb, III-Ia, III-Ic, III-IIa, II-IIIa, II-IIIb and II-IIId the HOMO is on isomer IV. In III-III1, III-III3, III-III4, III-III7, II-IIIe and III-IIb, the HOMO is on isomer III. Therefore the ionization would be expected to occur at these orbitals. In Table 5.9 the distribution of ChelpG charges in cation dimers for each monomer are shown. It can be easily seen that charges are dominantly accommodated on isomer IV and isomer II.

Table 5.8. The location of HOMO orbitals in the neutral $(C_3H_6N_6O_6)_2$ dimers on a monomer basis are shown. Single tick- marks indicate that the electron is merely one monomer and double tick-marks indicate that the electron is localized on two monomers.

Dimers	**Isomer I**	**Isomer II**	**Isomer III**	**Isomer V**	**Isomer IV**
I-Ik	√√				
I-I4	√				
I-I7	√				
I-I8	√				
II-IIa		√			
II-IIc		√			
II-IIq		√			
II-II4		√			
II-II5		√			
II-IIv		√			
II-II2z		√			
II-IIw		√			
III-III1			√		
III-III3			√		
III-III4			√		
III-III7					√
III-III9					√√
I-IIa		√			
I-IIb	√				
II-Ia		√			
II-Ib		√			
II-Ic		√			
I-IIIb					√
I-IIIc	√				
I-III	√				
III-Ia					√
III-Ic					√
II-IIIa					√
II-IIIb					√
II-IIId					√
II-IIIe			√		
III-IIa					√
III-IIb			√		

Table 5.9. ChelpG charges on each conformer in the $(C_3H_6N_6O_6)_2$ dimers.

Cations of the dimers	IsomerI	IsomerII	IsomerIII	Isomer V	Isomer IV
I-Ik	0.74			0.26	
I-I4	0.26	0.74			
I-I7	0.73/0.27				
I-I8	0.29	0.71			
II-IIa	0.24	0.76			
II-IIc	0.72			0.28	
II-IIq		0.74		0.26	
II-IIv	0.29	0.71			
II-II2z	0.77/0.23				
II-IIw	0.27	0.73			
III-III1			0.79		0.21
III-III3			0.79		0.21
III-III4			0.11		0.89
III-III7			0.79		0.11
III-III9			0.13		0.87
I-IIIb	0.14				0.86
I-IIIc		0.75	0.25		
I-III		0.76	0.24		
III-Ia				0.06	0.94
III-Ic	0.13				0.87
I-IIa		0.74		0.26	
I-IIb	0.26	0.74			
II-Ia	0.29	0.71			
II-Ib	0.29	0.71			
II-Ic	0.27	0.73			
II-IIIa				0.09	0.91
II-IIIb		0.89		0.11	
II-IIId				0.10	0.90
II-IIIe			0.75	0.15	
III-IIa	0.14				0.86
III-IIb	0.18		0.82		

Isomer V is not a preferable conformer for the charge accommodation possibly due to orbital energy differences. Isomer I and isomer III bear the charges with similar probability. The ChelpG charge analysis of the cations show that 59% of the complexes developed more than 70% of the +1 charge on the isomer where the neutral state HOMO was located. The remaining 41% went through ionization induced structural changes and therefore an isomeric charge/orbital match up is no longer possible. The neutrals where the HOMO was on isomer IV lost the electron and developed 90% of the positive charge. The

Cation dimers	δ_H	C-H	O-H
I-I8(II-I)	0.069	1.169	1.700
II-IIa(II-I)	0.093	1.152	1.824
II-II2z	0.109	1.171	1.709
I-I4(I-II)	0.127	1.203	1.559
II-Ic	0.128	1.179	1.647
II-IIw(I-II)	0.13	1.179	1.647
I-Ik(V-II)	0.163	1.183	1.633
II-IIq(V-II)	0.179	1.217	1.523
I-IIa(V-II)	0.179	1.217	1.521
II-IIv(I-II)	0.186	1.217	1.513
I-IIb(II-I)	0.186	1.180	1.647
II-Ia	0.186	1.217	1.514
I-III(III-II)	0.201	1.217	1.529
I-IIIc(II-III)	0.232	1.231	1.492

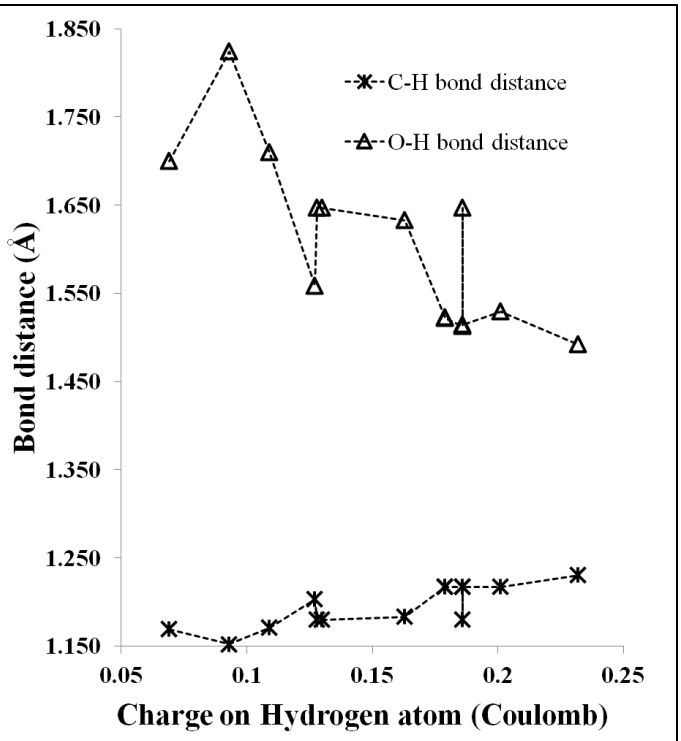

(a)

Cation dimers	δ_o	C-H	O-H
I-IIIc(II-III)	-0.445	1.231	1.492
I-III(III-II)	-0.435	1.217	1.529
I-I4(I-II)	-0.398	1.203	1.559
I-Ik(V-II)	-0.387	1.183	1.633
II-IIq(V-II)	-0.374	1.217	1.523
I-IIa(V-II)	-0.374	1.217	1.521
II-IIv(I-II)	-0.37	1.217	1.513
II-IIw(I-II)	-0.37	1.179	1.647
I-IIb(II-I)	-0.37	1.180	1.647
II-Ia	-0.37	1.217	1.514
II-Ic	-0.369	1.179	1.647
II-IIa(II-I)	-0.36	1.152	1.824
I-I8(II-I)	-0.353	1.169	1.700
II-II2z	-0.308	1.171	1.709

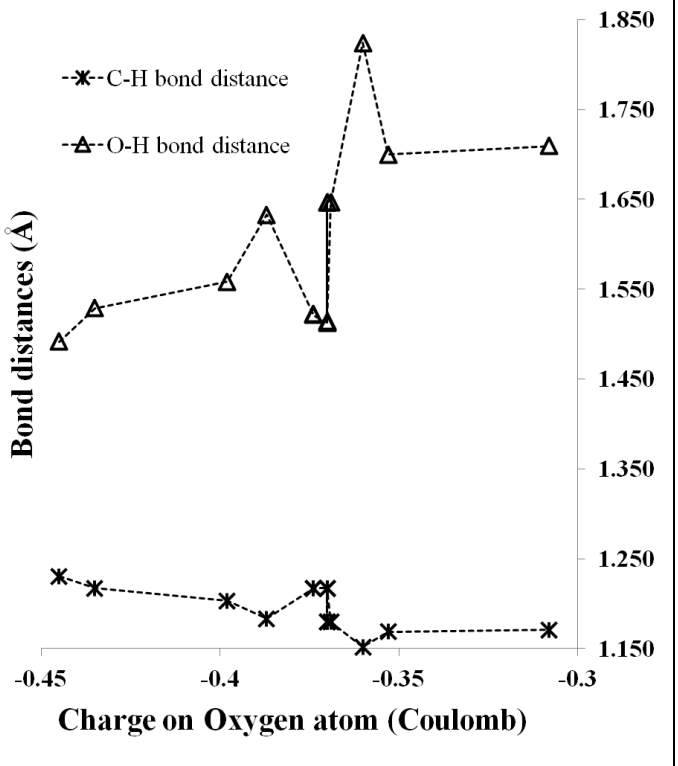

(b)

Figure 5.14. Distribution of charge of atoms versus bond distances in cation complexes. (a) Charge on hydrogen atom versus C-H and O-H bond distances. (b) Charge on oxygen atoms versus C-H and O-H bond distances.

cations where the charge is localized on the isomers I, II and III kept only 70-80% of the charge, and the rest of the charge was on the partner isomer. When functional groups are considered, in all cations the charge was mostly on the nitrogen atoms of the -NO_2 groups. This is in accord with previous experimental studies [32, 33] which showed that the -NO_2 groups were where the ionization and other photochemical events took place in nitramine energetic materials such as the monomer $C_3H_6N_6O_6$.

In Figure 5.14 the distribution of atomic charges versus bond distances in the cation complexes in which the $C^{-\delta}\cdots H^{+}\cdots{}^{-\delta}ON$ formation was observed are shown. The was done to see whether this three-atom interaction could be called a H-bonding. For that to occur, a substantial negative charge on O and positive charge on H had to be accumulated. In plot (a) (top) the charges on hydrogen atoms versus C-H and O-H bond distances are plotted and in plot (b) (bottom) the charges on oxygen atoms versus C-H and O-H bond distances are plotted. The values for each dimer are given at the left handside of the plots. While the C-H distances increase charges on hydrogen atom also increase but O-H intermolecular distances decrease. While C-H bond distances get longer the oxygen atoms build up negative charge and the O-H intermolecular distances shorten. However we never encounter a full +1 charge on H or a full -1 charge on O. Clearly this formation can not be classified as a H-bond.

5.4. Frequency Distributions in the Neutral $(C_3H_6N_6O_6)_2$: Vibrational Excitation

The frequencies of the neutral complexes were multiplied by 0.964 to scale for the B3LYP/6-31+G(d,p) method. They were then grouped in frequency intervals of 100 cm^{-1} and the number of frequencies within an interval were counted. The five complexes that represent the different distributions observed among the 33 neutral complexes were shown in Figure 5.15.

Most of the vibrations are within the 0-100 cm^{-1} frequency interval. In this interval more than 10% of the total of 120 vibrations are accumulated and the complexes that contain isomer II have the highest number of vibrations. All complexes belong to the C_1 point group therefore all vibrations can be excited by at least one quantum. At room

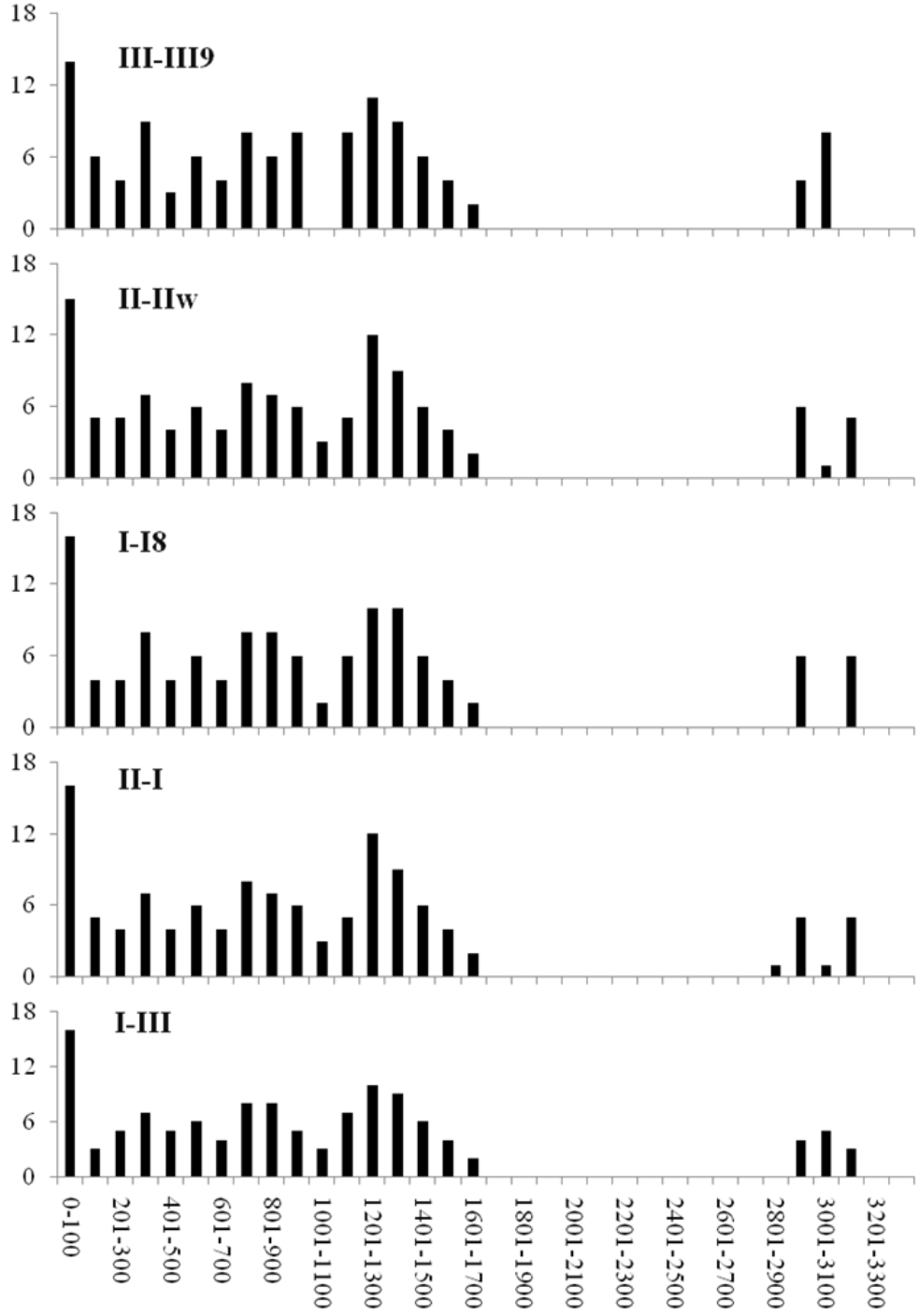

Figure 5.15. Vibrational frequency distributions in representative neutral complexes per 100 cm^{-1} intervals.

temperature, all of the vibrations within the 0-200 cm^{-1} interval can be excited. These vibrations are the relative motion of the two isomers making up the complex, rotation of the -NO_2 groups with respect to the ring system, and ring breathing modes. Excitation of

these vibrations, which are most likely to be anharmonic in nature, will result in dissociation of the complex back into its isomers, release of the NO_2 groups from the rings, and dissociation of the ring system. Such mechanisms have already been suggested to occur in the experimental studies on the ionization and thermal decomposition of the $C_3H_6N_6O_6$ molecule [21-28, 30-33].

The vibrational frequencies in the 1200 and 1300 cm^{-1} interval belong to the ring N-C-N bending modes. The dimers containing isomer II have a steeper frequency distribution in this interval due to its different structural characteristics. The effect of isomer II on the frequency distribution within this interval can be seen more clearly by a comparison of the distributions of the I-II and I-III. This example highlights the fact that even though the complexes may be formed by combination of different isomers, each isomer within the complex preserves its nuclear and electronic structure. As a result, upon energetic stimulation the complex would preferentially separate back into the isomers making it up and depending on the form of the excitation, the ring systems would be compromised.

The C-H bond stretch modes are within the 2900-3200 cm^{-1} interval. The frequency distributions in this interval are a convolution of the frequency distributions of the individual isomers making up the complex. This would be expected since the C-H vibration is isolated. i.e. not affected by the interaction of the isomer it is observed in with the other isomer in the complex.

5.5. Dipole moments of $(C_3H_6N_6O_6)_2$: Possibilities of further clustering

Clustering occurs initially through long-range interactions. In the $(C_3H_6N_6O_6)_2$ dimers the strongest long-range interaction is the dipole-dipole interaction. Where two monomers could align their dipoles at initial encounter, an already formed neutral dimer with a large dipole moment could attract another monomer with a dipole moment in the absence of other stimulating energetic factors. A neutral dimer that formed may not have a dipole moment when neutral but it may have a large dipole moment in the cationic state. The cation could then be solvated other neutrals and stabilize or reactions could ensue.

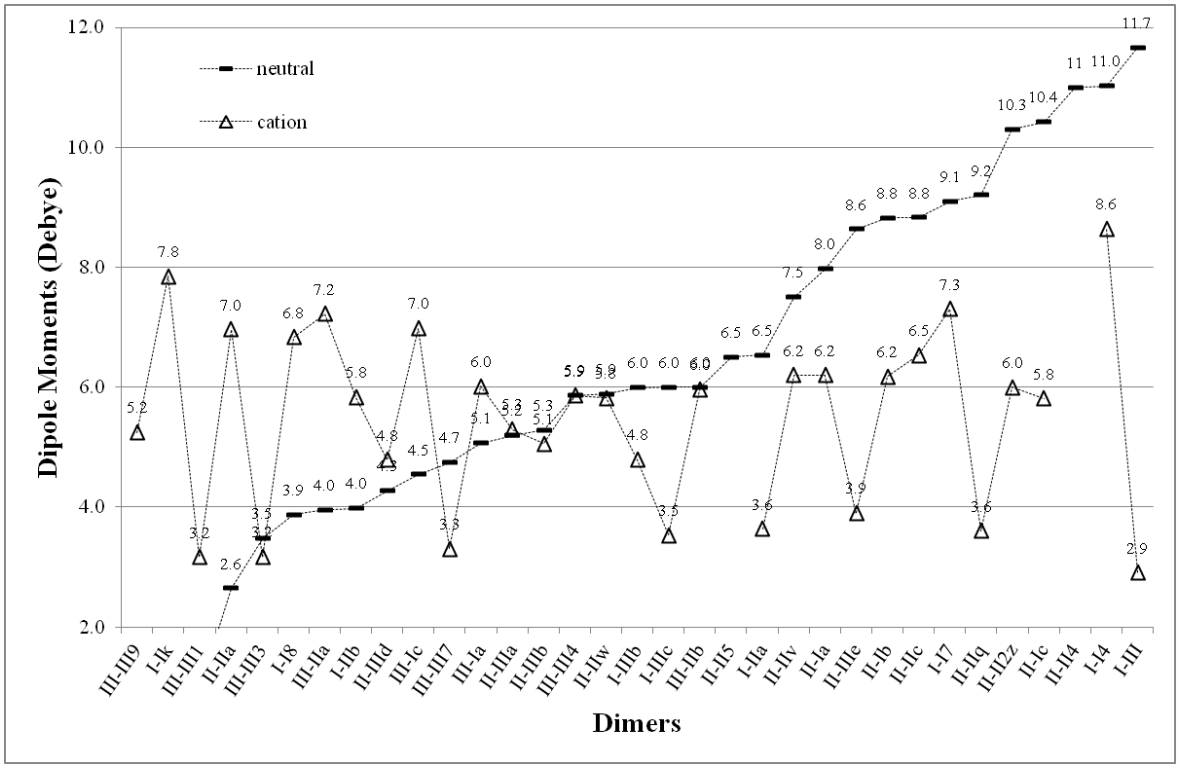

Figure 5.16. Dipole moments of neutral and cation dimers.

The dipole moments of the neutral and cationic dimers are shown in Figure 5.16. The dimers in the x-axis have been ordered according to their dipole moments in the neutral state. While the neutrals with isomer III have low dipole moments, those with isomer II have high dipole moments. Due to extensive structural changes in ionization, there is no correlation between the dipole moments of the cations and the neutrals they originated from. Concentrating on the five most probable dimers that can be encountered, namely, I-IIIc, III-III9, III-III3, and II-IIId, we see that the III-III9 neutral has no dipole moment and I-IIIc has the highest dipole moment of 6.0 Debye. The III-III3 and II-IIId are between the two. Based on magnitudes of the dipole moments, one could say that I-IIIc dimer has the potential for further clustering. According to Figure 5.16, had the III-III9 neutral been ionized and went through the same structural changes as encountered in the optimizations, there would be a jump of dipole moment from 0 to 5.2 Debye which could increase its potential for further clustering. It should be recognized, however, that in addition to the magnitudes, the orientation of the dipole vectors matter in cluster formation and repulsive steric effects could prevent alignment. For definitive answers, more experiments and a detailed computational study would have to be undertaken.

6. CONCLUSIONS

Structure search for dimeric forms of $C_3H_6N_6O_6$, conducted using the B3LYP/6-31+G(d,p) method, has produced 33 local minima for the $(C_3H_6N_6O_6)_2$ dimers. The complexation energies and relative energies were corrected for the basis set superposition error which was around 9-11 kJ/mol maximum (25-30% of the complexation energies) for dimers in which both monomers contributed to the molecular orbitals and was 5.6 kJ/mol (20% of the complexation energy) minimum. All complexation processes yielded negative complexation energies, indicating that the complexation is exothermic. The corrected complexation energies range between -1.5 to -30.6 kJ/mol. No charge transfer from one monomer to the other was observed in the neutral dimers. The dimers with electron density on both monomers had the largest complexation energy. Based on the complexation energies and relative energies, four of these neutrals were highlighted as the most probable candidates, I-IIIc, III-III9, III-III3, and II-IIId.

A majority of the clusters were formed between low energy isomers of the monomer, however, those with the lowest relative energies shared a common monomer, IV, that is higher in energy than the three monomers used to construct the dimers. The HOMO of monomer IV has the largest electronic extent which has a stabilizing effect during dimerization. The structures, orbitals and charges and frequency distributions indicate that there is no drastic change in the structure of the monomers while in the dimer. While thermodynamically stable, having more than 10% of their vibrational frequencies within the 0-200 cm^{-1} interval, the dimers can dissociate into intact monomers upon heating.

When ionized, major structural reconstruction takes place, including NO_2 expulsion and proton abstraction through which the dimer becomes a proton-bound complex. It was peculiar that none of the dimers went through both. The latter process caused HONO formation in one of the cations, II-IIIb, which was stabilized by more than 100 kJ/mol compared to the other cations in the set. These observations are in accord with the experiments pertaining to the $C_3H_6N_6O_6$ monomer, even though the conformational form of the monomer is not specified. This study shows that the dissociative tendency of the $C_3H_6N_6O_6$ continues within the dimer however the pathway chosen depends on the

configuration of the -NO_2 functional group orientation on the ring system and the boat-chair preference of the ring system of the $C_3H_6N_6O_6$.

Charge distributions of the dimer cations revealed that at least 70% of the +1 charge was localized on one monomer. As confirmed by center-of-mass distance analysis, this charge localization causes the monomers to approach each other due to charge-dipole interactions and more favorable orientational arrangements due to functional group expulsion.

The ionization potentials range from an adiabatic value of 9.4 eV to a vertical value of 9.8 eV. Clustering lowers the adiabatic ionization energy due to solvation stabilization of one monomer by the other. The 0.4 eV difference between the adiabatic and vertical ionization potentials is a result of the relaxation of the dimer due to the structural rearrangements induced upon ionization.

REFERENCES

1. Montgomery Jr., J. A. and H. H. Michels, "Structure and stability of trinitramide", *The Journal of Physical Chemistry*, Vol. 97, No. 26, pp. 6774–6775, 1993.

2. Lee C. K. M., and K. M. Stenstorm, *Competitive Adsorption of Cyclotrimethylenetrinitramine (RDX) and Cyclotetramethylenetetranitramine (HMX)*, UCLA ENG 96-152, Civil and Environmental Engineering Department, University of California at Los Angeles, Los Angeles, 1996.

3. Merchant, M. and S. R., Weinberger, "Recent advancements in surface-enhanced laser desorption/ionization-time of flight-mass spectrometry", *Electrophoresis*, Vol. 21, No.6, pp. 1164–1177, 2000.

4. Karas M. and R. Krüger, "Ion Formation in MALDI: The Cluster Ionization Mechanism", *Chemical Reviews*, Vol. 103, No. 2, pp. 427–440, 2003

5. Beavis R. C. and B. T. Chait, "Velocity distributions of intact high mass polypeptide molecule ions produced by matrix assisted laser desorption", *Chemical Physics Letters*, Vol. 181, No. 5, pp. 479-484, 1991.

6. Ehring, H., M. Karas and F. Hillenkamp, "Role of photoionization and photochemistry in ionization processes of organic molecules and relevance for matrix-assisted laser desorption lonization mass spectrometry", *Organic Mass Spectrometry*, Vol. 27, No. 5, pp. 472-480, 1992.

7. Zenobi, R. and R. Knochenmuss,"Ion Formation in MALDI, Mass Spectrometry", *Mass Spectrometry Reviews*, Vol. 17, No. 5, pp. 337–366, 1998.

8. Meffert A. and J. Grotemeyer, "Dissociative proton transfer in cluster ions: clusters of aromatic carboxylic acids with amino acids", *International Journal of Mass Spectrometry*, Vol. 210, No. 1-3, pp. 521-530.

9. Knochenmus R. and A. Vertes, "Time-delayed 2-Pulse Studies of MALDI Matrix Ionization Mechanisms", *The Journal of Physical Chemistry B*, Vol. 104, No. 23, pp. 5406-5410, 2000.

10. Ledingham, K.W.D. and R.P. Singhal, "High Intensity Laser Mass Spectrometry — A Review", *International Journal of Mass Spectrometry and Ion Processes*, Vol. 163, No. 3, pp. 149-168, 1997.

11. Hankin, S. M., A. D. Tasker, L. Robson, K. W. D. Ledingham, X. Fang, P. McKenna, T. McCanny, R. P. Singhal, C. Kosmidis, P. Tzallas, D. A. Jaroszynski, D. R. Jones, R. C. Issac, S. Jamison, "Femtosecond laser time-of-flight mass spectrometry of labile molecular analytes: laser-desorbed nitro-aromatic molecules", *Rapid Communications in Mass Spectrometry*, Vol. 16, No. 2, pp. 111-116, 2002.

12. Dikmelik, Y., C. McEnnis and J. B. Spicer, "Femtosecond-laser-induced breakdown spectroscopy of explosives", *Detection and Remediation Technologies for Mines and Minelike Targets XI*, Vol. 6217, pp. 62172A, 2006.

13. McEnnis C., Y. Dikmelik and J. B. Spicer, "Femtosecond laser-induced fragmentation and cluster formation studies of solid phase trinitrotoluene using time-of-flight mass spectrometry", *Applied Surface Science*, Vol. 254, No. 2, pp. 557-562, 2007.

14. Dimov, S.S. and S.L. Chryssoulis, "A comparative study on detection of organic surface modifiers on mineral grains by TOF-SIMS, VUV SALI TOF-SIMS and VUV SALI with laser desorption", *Applied Surface Science*, Vol. 231-232, pp. 528-532, 2004.

15. Schuhle U., J. B. Pallix and C. H. Becker, "Sensitive mass spectrometry of molecular adsorbates by stimulated desorption and single-photon ionization", *Journal of the American Chemical Society*, Vol. 110, No. 7, pp. 2323-2324, 1988.

16. Lykke K. R., P. Wurz, D. H. Parker, M. J. Pellin, "Molecular Analysis by Ionization of Laser-Desorbed Neutral Species", *Applied Optics*, Vol. 32, No. 6, pp. 857-866, 1993.

17. Becker C. H. and K. T. Gillen , "Surface analysis by nonresonant multiphoton ionization of desorbed or sputtered species", *Analytical Chemistry*, Vol. 56, No. 9, pp. 1671-1674, 1984.

18. Weickhardt, C. and K. Tönnies, "Short pulse laser mass spectrometry of nitrotoluenes: ionization and fragmentation behavior", *Rapid Communications in Mass Spectrometry*, Vol.16, No. 5, pp. 442-446, 2002.

19. Mullen C., A. Irwin, B. V. Pond, D. L. Huestis, M. J. Coggiola, H. Oser, "Detection of Explosives and Explosives-Related Compounds by Single Photon Laser Ionization Time-of-Flight Mass Spectrometry", *Analytical Chemistry*, Vol. 78, No. 11, pp. 3807-3814, 2006.

20. Gross J. H., *Mass spectrometry: A textbook*, Springer-Verlag, Berlin, 2004.

21. Stals J., "Chemistry of Aliphatic Unconjugated Nitramines Part 7.-Interrelations between the Thermal, Photochemical and Mass Spectral Fragmentation of RDX", *Transactions of the Faraday Society*, Vol. 67, pp. 1768-1775, 1971.

22. Bradley J. N., A. K. Butler, W. D. Capey, J. R. Gilbert, "Mass Spectrometric Study of the Thermal Decomposition of 1,3,5-trinitrohexahydro-1,3,5-triazine (RDX) ", *Journal of the Chemical Society, Faraday Transactions 1*, Vol. 73, No. 0, pp. 1789-1795, 1977.

23. Farber M., "Mass spectrometric investigations of the thermal decomposition of 1,3,5,7-tetranitro-l,3,5,7-tetraazacylooctane (HMX) and 1,3,5-trinitro-1,3,5-triazacyclohexane (RDX) ", *Mass Spectrometry Reviews*, Vol. 11, pp. 137-152, 1992.

24. Gillis R. G., M. J. Lacey and J. S. Shannon, "Chemical Ionisation Mass Spectra of explosives", *Organic Mass Spectrometry*, Vol. 9, No. 3, pp. 359-364, 1974.

25. Yinon J., D. J. Harvan and J. R. Hass, "Mass Spectral Fragmentation Pathways in RDX and HMX. A Mass Analyzed Ion Kinetic Energy Spectrometric/Collisional Induced Dissociation Study", *Organic Mass Spectrometry*, Vol. 17, No. 7, pp. 321-326, 1982.

26. Yinon J., "Mass Spectral Fragmentation Pathways in 2,4,6-Trinitroaromatic Compounds. A Tandem Mass Spectrometric Collision Induced Dissociation Study", *Organic Mass Spectrometry*, Vol. 22, No. 8, pp. 501-505, 1987.

27. Zhao X., E. J. Hintsa and Y.T. Lee, "Infrared Multiphoton Dissociation of RDX in a Molecular Beam", *Journal of Chemical Physics*, Vol. 88, No. 2, pp. 801-810, 1988.

28. Snyder A. P., J. H. Kremer, S. A. Liebman, M. A. Schroeder, R. A. Fifer, "Characterization of Cyclotrimethylenetrinitramine (RDX) by N,H Isotope Analyses with Pyrolysis-Atmospheric Pressure Ionization Tandem Mass Spectrometry", *Organic Mass Spectrometry*, Vol. 24, No. 1, pp. 15-21, 1989.

29. Choi M., H. Kim and C. Chung, "FT-IR Spectra of Photochemical Reaction Products of Crystalline RDX", *The Journal of Physical Chemistry*, Vol. 99, No. 43, pp. 15785-15789, 1995.

30. Cabalo J. and R. Sausa, "Detection of Hexahydro-1,3,5-trinitro-1,3,5-triazine (RDX) by Laser Surface Photofragmentation–Fragment Detection Spectroscopy", *Applied Spectroscopy*, Vol. 57, No. 9, pp. 1196-1199, 2003.

31. Maharrey S. and R., Jr. Behrens, "Thermal Decomposition of Energetic Materials. 5. Reaction Processes of 1,3,5-Trinitrohexahydro-s-triazine below its Melting Point", *The Journal of Physical Chemistry A*, Vol. 109, No. 49, pp. 11236-11249, 2005.

32. Guo Y. Q., M. Greenfield and E. R. Bernstein, "Decomposition of Nitramine Energetic Materials in Excited Electronic States: RDX and HMX", *Journal of Chemical Physics*, Vol. 122, No. 24, pp. 244310, 2005.

33. Greenfield M., Y.Q. Guo and E.R. Bernstein, "Ultrafast Photodissociation Dynamics Of HMX and RDX from their Excited Electronic States via Femtosecond Laser Pump–Probe Techniques", *Chemical Physics Letters*, Vol. 430, No. 4-6, pp. 277-281, 2006.

34. Politzer P. and M. Yuguang, "Noncovalent Intermolecular Energetics: RDX Crystal", *International Journal of Quantum Chemistry*, Vol. 100, No. 5, pp. 733-739, 2004.

35. Okovytyy S., Y. Kholod, M. Qasim, H. Fredrickson, J. Leszczynski, "The Mechanism of Unimolecular Decomposition of 2,4,6,8,10,12-Hexanitro-

2,4,6,8,10,12-hexaazaisowurtzitane. A Computational DFT Study", *The Journal of Physical Chemistry A*, Vol. 109, No. 12, pp. 2964-2970, 2005.

36. Chakraborty D., R. P. Muller, S. Dasgupta, W. A. Goddard III, "Mechanism for Unimolecular Decomposition of HMX (1,3,5,7-Tetranitro-1,3,5,7-tetrazocine), an ab Initio Study", *The Journal of Physical Chemistry A*, Vol. 105, No. 8, pp. 1302-1314, 2001.

37. Brill T. B., M. C. Beckstead, J. E. Flanagan, M. C. Lin, T. A. Litzinger, R. H. W. Waesche, C. A. Wight, "Chemical Speciation and Dynamics in the Surface Combustion Zone of Energetic Materials", *Journal of Propolsion and Power*, Vol. 18, No. 4, pp. 824-834, 2002.

38. Lyman J.L., Y.C. Liau and H. V. Brand, "Thermochemical Functions for Gas-Phase, 1,3,5,7-Tetranitro-1,3,5,7-tetraazacyclooctane (HMX), its Condensed Phases, and its Larger Reaction Products", *Combustion and Flame*, Vol. 130, No. 3, pp. 185–203, 2002.

39. Lewis J.P., "Energetics Of Intermolecular HONO Formation in Condensed-Phase Octahydro-1,3,5,7-Tetranitro-1,3,5,7-Tetrazocine (HMX)", *Chemical Physics Letters*, Vol. 371, No. 5-6, pp. 588–593, 2003.

40. Tsiaousis D., R.W. Munn, P.J. Smith, P.L.A. Popelier, "Polarizability of Acetanilide and RDX in the Crystal: Effect of Molecular Geometry", *Chemical Physics*, Vol. 305, No. 1-3, pp. 317–323, 2004.

41. Rice B.M. and E.F.C. Byrd, "Theoretical chemical characterization of energetic materials", *Journal of Materials Research*, Vol. 21, No. 10, pp. 2444-2452, 2006.

42. Byrd E.F.C., G. E. Scuseria and C. F. Chabalowski, "An ab Initio Study of Solid Nitromethane, HMX, RDX, and CL20: Successes and Failures of DFT", *The Journal of Physical Chemistry B*, Vol. 108, No. 35, pp. 13100-13106, 2004.

43. White J.D., F. A. Akin, H. Oser, D. R. Crosley, "Production of the NO Photofragment in the Desorption of RDX and HMX from Surfaces", *Applied Optics*, Vol. 50, No. 1, pp. 74-81, 2011.

44. Weickhardt C., U. Boesl and E. W. Schlag, "Laser Mass Spectrometry for Time-Resolved Multicomponent Analysis of Exhaust Gas, '*Analytical Chemistry*", Vol. 66, No. 7, pp. 1062-1069, 1994.

45. Matsumoto J., C. H. Lin and T. Imasaka, "Supersonic Jet Multiphoton Ionization Mass Spectrometry Using Nanosecond and Femtosecond Pulse Lasers", *Analytica Chimica Acta*, Vol. 343, No. 1-2, pp. 129-133, 1997.

46. Shen Y. C., T. Lo, P. F. Taday, B. E. Cole, W. R. Tribe, M. C. Kemp, "Detection and identification of explosives using terahertz pulsed spectroscopic imaging", *Applied Physics Letters*, Vol. 86, No. 24, pp. 241116-241118, 2005.

47. Cook D. J., B. K. Decker, G. Maislin, M. G. Allen, "Through Container Thz Sensing: Applications for Explosives Screening", *Terahertz and Gigahertz Electronics and Photonics III*, Vol. 5354, pp. 55-62, 2004.

48. Chen Y., H. Liu, Y. Deng, D.B. Veksler, M. S. Shur, X.C. Zhang, D. Schauki, M. J. Fitch, R. Osiander, C. Dodson and J. B. Spicer, "Spectroscopic characterization of explosives in the far-infrared region", *Terahertz for Military and Security Applications II*, Vol. 5411, No. 1, pp. 1-8, 2004.

49. McEnnis C., Y. Dikmelik, T. J. Cornish, M. D. Antoine, P. A. Demirev, J. B. Spicer, "Investigation of the Fragmentation of Explosives by Femtosecond Laser Mass Spectrometry", *Detection and Remediation Technologies for Mines and Minelike Targets XI*, Vol. 6217, No. 1, pp. 621729, 2006.

50. Harris N. J. and K. Lammertsma, "Ab Initio Density Functional Computations of Conformations and Bond Dissociation Energies for Hexahydro-1,3,5-trinitro-1,3,5-triazine", *Journal of the American Chemical Society*, Vol. 119, No.28, pp. 6583-6589, 1997.

51. Levine, I. R., *Quantum Chemistry*, Sixth Edition, Pearson Education, Inc., New York, USA, 2009.

52. Hohenberg P. and W. Kohn, "Inhomogeneous Electron Gas", *Physical Review*, Vol. 136, No. 3B, pp. B864-B871, 1964.

53. Chong D. P., *Recent Advances in Density Functional Methods Part II*, World Scientific Publishing Co. Inc, Singapore 1997.

54. Parr, R. G. and W. Yang, *Density-Functional Theory of Atoms and Molecules*, Oxford University Press, New York, 1989.

55. W. Koch and M. C. Holthausen, *A Chemist's Guide to Density Functional Theory*, Second Edition, Wiley-VCH Verlag, Weinheim, 2000.

56. Kohn W. and L. J. Sham, "Self-Consistent Equations Including Exchange and Correlation Effects", *Physical Review*, Vol. 140, No. 4A, pp. A1133-A1138, 1965.

57. Jensen F., *Introduction to Computational Chemistry*, Second Edition, John Wiley & Sons Ltd., West Sussex, 2007.

58. Ortiz G. and P. Ballone, "Pseudopotentials for Non-Local-Density Functionals", *Physical Review B*, Vol. 43, No. 8, pp. 6376-6387, 1991.

59. Becke, A. D., "A New Mixing of Hartree-Fock and Local Density Functional Theories", *The Journal of Chemical Physics*, Vol. 98, No. 2, pp. 1372-1377, 1993.

60. Lee, C., W. Yang and R. G. Parr, "Development of Colle-Salvatti Correlation Energy Formula into a Functional of the Electron Density", Physical Review B, Vol. 37, No. 2, pp. 785-789, 1988.

61. Becke, A. D., "Density Functional Thermochemistry. III. The Role of Exact Exchange", *The Journal of Chemical Physics*, Vol. 98, No. 7, pp. 5648-5652, 1993.

62. Pauling, L. J., "The Nature of the Chemical Bond. IV. The Energy of Single Bonds and the Relative Electronegativity of Atoms", *Journal of American Chemical Society*, Vol. 54, pp. 3570-3582, 1932.

63. Cramer, C. J., *Essentials of Computational Chemistry: Theories and Models*, Second Edition, John Wiley & Sons Ltd., Chichester, 2007.

64. Foresman, J. B. and Æ. Frisch, *Exploring Chemistry with Electronic Structure Methods*, Second Edition, Gaussian, Inc., Pittsburgh, 1996.

65. Hehre, W. J., A *Guide to Molecular Mechanics and Quantum Chemical Calculations*, Wavefunction, Inc., Irvine, 2003.

66. Frisch M. J., G. W. Trucks, H. B. Schlegel, G. E. Scuseria, M. A. Robb, J. R. Cheeseman, J. A. Montgomery, Jr., T. Vreven, K. N. Kudin, J. C. Burant, J. M. Millam, S. S. Iyengar, J. Tomasi, V. Barone, B. Mennucci, M. Cossi, G. Scalmani, N. Rega, G. A. Petersson, H. Nakatsuji, M. Hada, M. Ehara, K. Toyota, R. Fukuda, J. Hasegawa, M. Ishida, T. Nakajima, Y. Honda, O. Kitao, H. Nakai, M. Klene, X. Li, J. E. Knox, H. P. Hratchian, J. B. Cross, V. Bakken, C. Adamo, J. Jaramillo, R. Gomperts, R. E. Stratmann, O. Yazyev, A. J. Austin, R. Cammi, C. Pomelli, J. W. Ochterski, P. Y. Ayala, K. Morokuma, G. A. Voth, P. Salvador, J. J. Dannenberg, V. G. Zakrzewski, S. Dapprich, A. D. Daniels, M. C. Strain, O. Farkas, D. K. Malick, A. D. Rabuck, K. Raghavachari, J. B. Foresman, J. V. Ortiz, Q. Cui, A. G. Baboul, S. Clifford, J. Cioslowski, B. B. Stefanov, G. Liu, A. Liashenko, P. Piskorz, I. Komaromi, R. L. Martin, D. J. Fox, T. Keith, M. A. Al-Laham, C. Y. Peng, A. Nanayakkara, M. Challacombe, P. M. W. Gill, B. Johnson, W. Chen, M. W. Wong, C. Gonzalez, and J. A. Pople, Gaussian 03, Revision D.01, Gaussian, Inc., Wallingford CT, 2004.

67. Breneman C. M. and K. B. Wiberg, "Determining atom-centered monopoles from molecular electrostatic potentials: the need for high sampling density in formamide conformational analysis", *Journal of Computational Chemistry*, Vol. 11, No. 3, pp. 361-373, 1990.

68. Lenzer, T., I. Yourshaw, M. R. Furlanetto, N. L.Pivonka, D. M. Neumark, "Zero electron kinetic energy spectroscopy of the $XeCl^-$ anion", *The Journal of Chemical Physics*, Vol. 116, No. 10, pp. 4170-4175, 2002.

69. Ferguson, M. J., G. Meloni, H. Gomez, D. M. Neumark, "Photoelectron spectroscopy of ClH_2^- and ClD_2^- : A probe of the $Cl+H_2$ van der Waals well and spin–orbit excited states", *The Journal of Chemical Physics*, Vol. 117, No. 18, pp. 8181-8184, 2002.

70. Neusser, H. J. and H. Krause, "Binding energy and structure of van der Waals complexes of benzene", *Chemical Reviews*, Vol. 94, No. 7, pp. 1829-1843, 1994.

71. Hagemeister, F. C., C. J. Gruenloh and T. S. Zwier, “Resonant ion-dip infrared spectroscopy of benzene-(water)$_n$-(methanol)$_m$ clusters with n + m = 4, 5”, *Chemical Physics*, Vol. 239, No. 1-3, pp. 83-96, 1998.

72. Shelley, M. Y., H. L. Dai, and T. Troxler, “Electronic relaxation and vibrational predissociation of benzene-acetylene van der Waals complexes”, *The Journal of Chemical Physics*, Vol. 110, No. 18, pp. 9081-9090, 1999.